The Pennsylvania State University

The Graduate School

Department of Mechanical and Nuclear Engineering

OPTIMIZATION OF HONEYCOMB CORE SANDWICH PANEL TO MITIGATE THE EFFECTS OF AIR BLAST LOADING

A Thesis in

Mechanical Engineering

by

Sumanta Kumar Nayak

Submitted in Partial Fulfillment
of the Requirements
for the Degree of

Master of Science

August 2010

The thesis of Sumanta Kumar Nayak was reviewed and approved* by the following:

Ashok D. Belegundu
Professor of Mechanical Engineering
Thesis Advisor

Panagiotis Michaleris
Associate Professor of Mechanical Engineering

Karen A. Thole
Professor of Mechanical Engineering
Head of the Department of Mechanical and Nuclear Engineering

*Signatures are on file in the Graduate School

ABSTRACT

Optimization of the honeycomb core sandwich panel to minimize the effects of air blast loading is analyzed and presented in this thesis. The sandwich panel consists of three layers in which honeycomb core is embedded in between two face plates. The honeycomb core has a great potential to absorb the impact energy of the blast by undergoing cyclic plastic buckling deformation. This energy absorption is not only influenced by the cell sizes but also by the face plate size and geometry which are essential in maximizing the energy absorption of the core by providing external supports. The core also stiffens the sandwich by maintaining larger gap between the face plates. So the main purposes of the core are to reduce the transmitted acceleration to the back plate and also to reduce the back face plate deformation. The optimization study investigates the size and shape of the face plates, and depth and cell size of the core. Mass of the sandwich and the maximum plastic strain of the face plates are constrained. The optimization is carried out in two different ways (I) response surface optimization and (II) direct optimization using Differential Evolution. In the response surface method Design Expert software is used to create response equations from the response values determined from sampled points based on central composite face centered design method. The response equations are used in FMINCON, a gradient based optimizer in MATLAB optimization toolbox, for optimization. Function evaluations are done using LS-DYNA. Honeycomb core is modeled as a continuum solid structure with equivalent mechanical properties. The equivalent mechanical properties are determined by virtual testing method and parameterized in terms of the important honeycomb cell parameters. The results obtained shows that stiffer front face plate minimizes the back face plate deformation and acceleration by effectively transferring the blast load to a larger area of the core. Low dense core is found to be suitable for minimizing the back face acceleration whereas relatively high dense and high depth core is found to be useful for minimizing the back face plate deformation. The results are compared with solid flat plate and with shape optimized solid plate of equal mass. Honeycomb core sandwich structure proves to be much more effective over a shape optimized solid plate of equal mass in reducing the transmitted acceleration.

TABLE OF CONTENTS

LIST OF FIGURES

LIST OF TABLES

LIST OF NOMENCLATURE

D	=	distance between opposite wall of honeycomb cell
t	=	thickness of honeycomb cell wall
h	=	honeycomb core depth
α	=	angle between honeycomb cell wall
$2H$	=	folding wavelength
$\mathbf{x}^{\mathbf{L}}$	=	lower limit on design variables
$\mathbf{x}^{\mathbf{U}}$	=	upper limit on design variables
$\mathbf{G}$	=	vector of x-, y-, z- coordinates of nodes in FE model
$\mathbf{q}^{i}$	=	i th velocity field or trial shape change vector
N_{dv}	=	Number of design variables
δ_b	=	Peak displacement of the back face plate center along z-direction relative to stiffener
a_b	=	Peak rigid body acceleration of the back face plate along z-direction
ε_{pmax}	=	Maximum effective plastic strain
t_f	=	thickness of the front face plate
t_b	=	thickness of the back face plate
s_f	=	bulge height in the front face plate
s_b	=	bulge height in the back face plate
M	=	total mass of the structure
M_f	=	mass of the front face plate
M_c	=	mass of the honeycomb core
M_b	=	mass of the back face plate
M_{st}	=	mass of the stiffener

ACKNOWLEDGEMENTS

I am highly grateful to my advisor Professor Ashok D Belegundu for his invaluable guidance and cooperation throughout this research, without which it would not have been feasible to accomplish this work. I would like to express my sincere thanks to him for allowing me to continue my thesis work even if I was away from the university campus to work in the Brookhaven National Laboratory. I can't forget his immense help to hold meetings in the weekends which was very convenient for me.

I specially thank to Anand Kumar Singh for executing the optimization code in the cluster and participating with me in numerous technical discussions in this research work. I also thank Vikas Argod and Rajeev Jain for their support at the early stage of this research. I thank Professor Panagiotis Michaleris for reviewing my thesis and providing valuable comments.

I express my deep thankfulness to my wife for her support and taking care my son while I was busy with this thesis work. Finally I thank my whole family for their encouragement, and I dedicate this thesis to them.

Chapter-1

INTRODUCTION

1.1 Motivation and thesis overview

Metal sandwich panels with cellular core (mostly honeycomb or aluminum foam) are finding increasing use over monolithic plates in structural design to withstand intense short duration pressure pulses, especially for blast and vehicle crash protection. The cellular core has the ability to absorb the impact energy of the pressure pulse by undergoing large plastic deformation at almost constant nominal stress. This characteristic of the cellular core results significant reduction in the transmitted acceleration and hence mitigates the damage causing potential of the blast impulse. Though metal sandwich panels have been used for a long time in aircraft and other light weight structures to maximize the bending stiffness per unit density, it has only be in recent years researchers have begun investigating the possible use of sandwich panels for blast protection. While the design optimization of monolithic structures for blast protection use have been studied well, metal sandwich panels are relatively less understood for blast mitigation.

This thesis investigates the optimization of the honeycomb core sandwich panel for minimizing the back face plate deformation and back face plate acceleration subjected to air blast loading. The sandwich panel consists of three layers in which honeycomb core is embedded in between two metal face plates. The honeycomb core which acts as sacrificing layer absorbs the impact energy of the blast by undergoing cyclic plastic buckling deformation. The energy absorption is not only influenced by the core material's mechanical properties but also by the geometric parameters defining the honeycomb core such as cell size, foil thickness, core depth and configuration of the cell. Face plates give external support to the honeycomb core and should maintain the structural integrity. For maximum benefit, the front face plate facing the blast should be able to transfer the blast impact to a larger area of the core and also deflect the blast wave. The former can be achieved by providing sufficient stiffness to the face plate and the latter

by giving a suitable shape to the face plate. The back face plate should have sufficient stiffness to provide the back support to the core. The challenge is to optimize the honeycomb core and face plate parameters simultaneously for maximizing the blast damage mitigation.

This optimization work involves both size and shape of the face plates and size of the honeycomb core. It involves an integration of an optimizer with LS-DYNA simulation code. The optimizer used for shape optimization of the aluminum monolithic plate for blast damage mitigation in our previous study [1] has been tailored to optimize the sandwich panel with honeycomb core. This optimization process is computationally very expensive, even on a parallel computer, as it uses the differential evolution optimization algorithm where the population evaluation for each generation involves finite element explicit analyses using LS-DYNA. For this reason a second approach based on response surface optimization has been implemented. Design Expert software is used to create response equations from the function values determined from sampled points based on central composite face centered design method. The response equations are used in FMINCON, a gradient based optimizer in MATLAB optimization toolbox, for optimization.

Finite element modeling of each hexagonal cell of a large honeycomb core panel in LS-DYNA will generate a prohibitive large number of nodes and degrees of freedom. Here, the core is modeled as a homogenized solid plate of equivalent mechanical properties, determined by virtual testing. Virtual testing is carried out in LS-DYNA to study the crush behavior (or load curve) of a unit honeycomb cell under quasi-static impact load. The effect of different geometric parameters describing the honeycomb core on its crush behavior is analyzed. Then all the relevant mechanical properties including the crush behavior is parameterized in terms of the most important honeycomb parameters. The mechanical property of the honeycomb core is modeled in LS-DYNA using the crushable foam model. The virtual testing results have been corroborated with available formulas in the literature.

1.2 Literature review

Earlier, a study carried out in our group by Vikas et al showed that the shape of a monolithic aluminum plate can be optimized to reduce dynamic displacement under blast [1]. They developed a robust methodology based on coupling Differential Evolution (DE) to LS-DYNA to minimize the plate's RMS displacement subjected to mass and maximum plastic strain constraint. The optimum shape had convex bulges on the front and back (front refers to charge side). This bulge deflects the blast and stiffens the plate, thereby mitigating the blast effect. The optimum shape also resulted smearing of plastic strain indicating the better utilization of material. Although the shaped plate performed very well compared to the flat plate, greater blast resistance can be offered by using sandwich structures. To take this research one step further, a study on the design of honeycomb sandwich structure for blast protection is carried out and presented in this thesis.

Xue and Hutchinson [3] compared the performance of sandwich panels (such as pyramidal truss core, square honeycomb and folded plate) to a solid plate of equal weight for blast resistance. They found that square honeycomb and folded plate outperformed the pyramidal truss core, but all three sandwich panels were capable of offering higher blast resistance compared to the solid plate. Further, the sandwich panels were found to be more effective in water than in air, due to fluid structure interaction. Limited optimization study was carried out, which did not consider material failure, shape and certain core parameters. Their study showed that sandwich panels are promising structures for blast resistance and more research should be carried out for their effective use. Fleck and Deshpande [4] developed an analytical methodology to analyze the dynamic response of metallic sandwich beams subject to both air and water blasts. Their finding on the basis of simple analytical formulas matched well with the result from Xue and Hutchinson's [3] three-dimensional FE calculations.

Yen, Skaggs and Cheeseman [5] carried out both experimental and computational analyses to study the effect of honeycomb crush strength on the dynamic response of a honeycomb core sandwich pendulum

system. The result indicated that total impulse of the system increased due to dishing (concave) deformation of the front face plate. Numerical results indicated that significant reduction in maximum stress amplitude propagating within the core can be achieved by suitable selection of honeycomb material with proper crush strength. It is understood that suitable shape of the front face plate can reduce the dishing deformation and hence the total blast impulse. Numerical analyses carried out in LS-DYNA using ConWep air blast function validated the experimental result. Hanssen et al [6] performed similar tests on aluminum foam core sandwich panels with results similar.

Main and Gazonas [7] investigated the uniaxial crushing of a cellular sandwich plate subjected to air blast. This study was aimed to mitigate the shock transmission by suitably distributing the mass among the face plates and the core for a given mass of the sandwich. Fluid structure interaction (FSI) has also been considered. It is stated that the capacity of sandwich plate to mitigate shock transmission is limited by the critical impulse requited to produce complete crushing (or densification mentioned in the paper) of the core. After complete crushing of the core, the stress (or shock) transmitted to the back face plate gets amplified. The shock mitigation can be improved by increasing the mass fraction of front face and the core. At the same time too much reduction in mass fraction of the back face plate leads to increased back face acceleration. So, an optimization study was carried out to find the optimal mass distribution to maximize the impulse absorption while limiting the back face acceleration. While this study considered the effect of face plate thicknesses and core depth in designing a sandwich plate for blast shock mitigation, it did not consider parameter related to the core.

Chi et al [8] experimented to study the effect of core height and face plate thicknesses on the response of honeycomb sandwich panels under blast loading. Experiments showed that prior to densification, the core provided structural support to the front plate and regulated the stress transferred to the back face plate. Once the onset of core densification starts, higher stresses are transferred to the back face plate which exhibited steeply increasing deflection. The impulse required for onset of core densification

increases with increase in core thickness. Deformation of face plate increases with decrease in its thickness and too much thinning results in tearing of the plates.

Zhu et al [9] shown that thick face plates with relative high density honeycomb core sandwich structure significantly reduces the back plate deformation subjected to blast and, for a given panel configuration, the back face deflection increases with impulse, approximately linearly. In their next paper Zhu et al [10] presented a limited optimal design study of the honeycomb sandwich panel. For same mass and exposed area (to the blast) of the panel, square size panel results maximum deformation of the face plates. The panel shows similar response with independent variation of the core density and the core height for a given mass of the panel. To keep the total mass constant, mass of the face plates is adjusted. For each case, optimum core density and core height is found. Karagiozova et al [11] carried out numerical analyses to prove the sandwich structure's potential application as a blast resisting structure. It states that the optimum sandwich configuration depends upon the applied blast load and, an optimum structure compromises between energy absorption of the core and the load transfer to the back face plate of sandwich. For same load, the acceleration of the back face plate depends upon its mass.

The results from all the research mentioned above indicates the sandwich structure's potential application as blast resisting structure. Most of the study explores the effect of different design parameters taken one at a time on the performance of the sandwich.

Yamashita and Gotoh [12] studied the impact behavior of honeycomb cells through numerical simulations and experiments. Numerical simulation using a single 'Y' cross-sectional model predicted the crush behavior, quite well, using appropriate boundary conditions at the edges. Crush strength increased with foil thickness and the branch angle. However highest crush strength per unit mass was obtained when cell shape is of regular hexagon. Changing the branch angle from 180^0 to 30^0 can result 1.5 times increase in crush strength, which implies that functionally gradient honeycomb material in crush strength can be fabricated by suitably changing the branch angle. Experiment shows that crush

strength increased with hammer travel which can be attributed to the air pressure enclosed in the honeycomb. Results from experiments with drop hammer velocity 10m/s and its corresponding quasi-static experiment are very similar. Wierzbicki [13] derived a simple formula from the basic principles of material continuity and plasticity for calculating the mean crush strength of metal honeycombs in terms of the cell diameter, foil thickness and the flow stress. The derivation is given for a general shape, and is then specified for a regular hexagon cell. The best value flow stress is found to be 0.7 times the ultimate stress. The result from this analytical solution is well matched to the experimental results. Zhang and Ashby [14] analyzed the collapse behavior of the honeycomb under both axial compression and in plane shear load. Buckling, debonding and fracture are identified as possible collapse mechanisms. For flexible honeycombs such as those made from Nomex, buckling and fracture are dominant mode of failure in simple axial compression test, but for rigid-plastic honeycombs (made from aluminum), buckling and plastic yielding dominates. Depth of the honeycomb has no effect and cell angle has little effect on out-of-plane strengths (compressive and shear). These strengths are highly sensitive to the density of the honeycomb. With increase in density, failure switches from buckling to debonding in shear and buckling to fracture in compression. It is also found that out-of-plane loading has little effect on in-plane failure and vice versa. For a given density, honeycomb shows greater axial strength than foams, but foams shows better heat insulation than honeycomb. Metal foam is a cellular structure consisting of a solid metal, and a large volume fraction of gas-filled pores. Wu and Jiang [15] performed both quasi-static and high speed impact (up to 28.14 m/s) crush test on six types honeycomb cellular structure. They mentioned that smaller cell size, short height honeycomb made from high strength material has high energy absorbing capacity. The test shows that crush strength is proportional to the initial striking velocity.

This research extends previous work by utilizing a formal optimization method in combination with LS-DYNA to optimize sizing parameters, shape of the both face plates and core properties while considering

material failure. The crush behavior of the honeycomb core which is relevant in this study is analyzed and parameterized in terms of the design variables.

Chapter 2

Homogenization of Honeycomb Structure via Virtual Testing

The honeycomb cells could be regular hexagon or any modified version of it such as OX type, reinforced hexagonal type, flex type, double-flex type and tube type [16]. Cell with four equal side faces is referred as square honeycomb. Each type has its special use in specific applications. The honeycomb core of different materials is commercially available. Some common materials are aluminum, fiberglass and Aramid fiber (Nomex, Kevlar and KOREX). Special honeycomb made from carbon and polyurethane is also available. In our study, Al5052 regular hexagon honeycomb cell is considered.

Finite element modeling of the honeycomb cellular core requires high density mesh to capture the cyclic plastic buckling deformation accurately under axial compressive loading. Element size along the depth of the honeycomb should be sufficiently small enough to allow the cyclic folding of the cell to take place as it would do in the experiment. However high element density leads to high computation time and iterative finite element analysis of honeycomb sandwich structure with hundreds of cells would be computationally impossible. Thus, it is the best to substitute the discrete honeycomb cellular core by a homogenized solid plate of equivalent mechanical properties. Here, homogenized properties are determined using virtual testing method. As the name implies, virtual testing is a computer based finite element analysis technique to replace expensive mechanical tests. A unit cell of the honeycomb is modeled in LS-DYNA.

2.1 Finite element modeling of the unit cell

Figures 2-1 and 2-2 show the hexagonal cell structure and its unit cell. The simplest repeating unit in this structure is a ‘Y’ shape, which is known as the unit cell. Unit cell has one side double wall and two side single walls. In double wall, two layers of foil are glued by adhesive. Finite element model of the unit cell is shown in Figure 2-4. The foil is modeled by quadrilateral Belytschko-Tsay shell elements, and the 0.01mm thick layer of adhesive at the double wall is modeled by solid elements. Symmetric boundary

conditions (B.Cs) are applied along all the edges of the foil (Figure 2-3), bottom areas are fixed and displacement load (crushing) is applied to an external rigid surface (like a drop hammer) which hits the top areas and moves with them. The main role of the top and bottom face plate is to contain the crushed honeycomb foil. In the actual mechanical test, a heavy steel hammer is used to crush the honeycomb. To replicate the actual test, the rigid surface is modeled using the rigid shell element and the mechanical properties are defined as that of steel but with a high fictitious density (Table 2-1). Al5052 aluminum alloy with bilinear isotropic-hardening inelastic material model is used for the foil (Table 2-1). Since the yield and ultimate strength of the Al5052 foil are very close, bilinear inelastic material model with very low tangent modulus is a reasonable approximation. For the adhesive, perfectly plastic material model is adopted (Table 2-1). Automatic single surface contact is applied to the model with sliding and sticking frictional coefficients equal to 0.2 and 0.3, respectively. These mechanical properties of the foil and the adhesive, and friction coefficient values are obtained from the literature [12]. All the tests are carried out at a hammer speed of 80 mm/s along the depth of the honeycomb, which can be considered as quasi-static tests since impact test involves very high hammer speeds in the order of m/s.

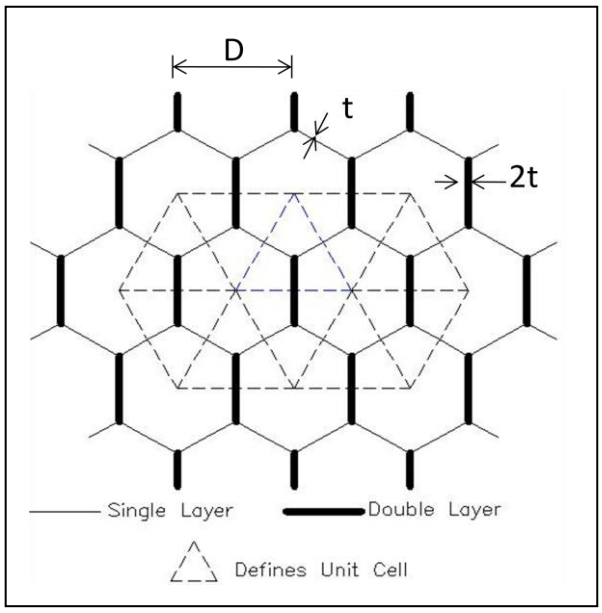

(a)

Figure **2-1**: Honeycomb cell geometry

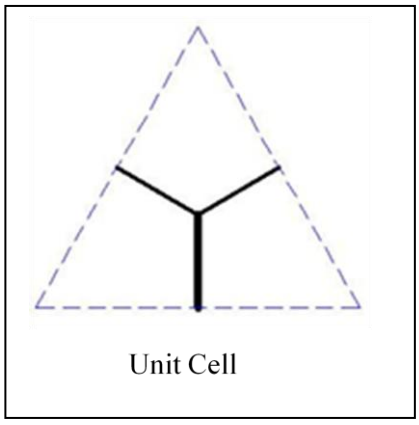

(b)

Figure **2-2**: Unit cell

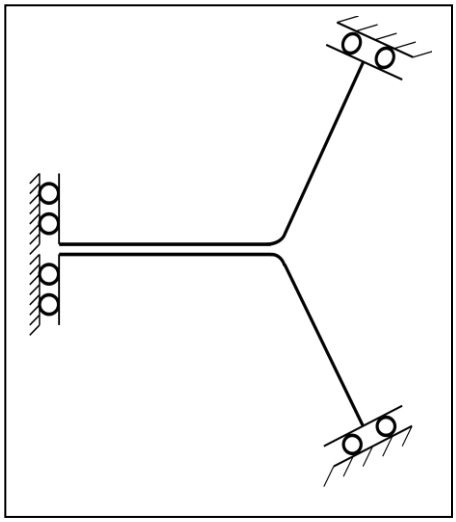

Figure **2-3**: Boundary conditions on the unit cell

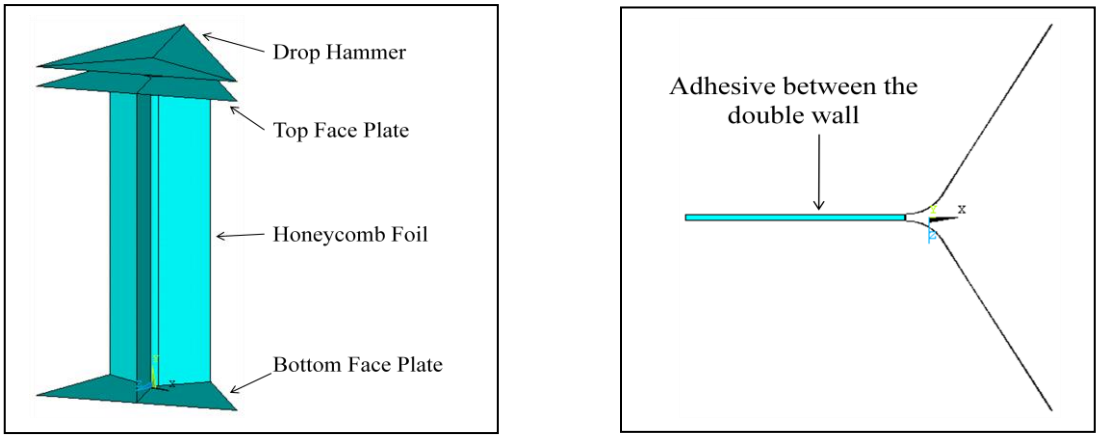

Figure **2-4**: Finite element model of the honeycomb unit cell

Table **2-1**: Material properties of the honeycomb unit cell model

Material	Density (kg/ m^3)	Young's Modulus (GPa)	Yield Stress (MPa)	Tangent Modulus (MPa)	Poison's Ratio
Foil-Al5052	2680	72	300	50	0.34
Adhesive	2000	5	30	0	0.3
Drop Hammer-Steel	288E5	200	-	-	0.24

2.2 Virtual testing results

Figure 2-5 and 2-6 shows a typical crushing phenomenon and its load curve obtained from the test. As the hammer travels, buckling of the foil starts from near the impact edge and propagates downward. Figure 2-6 shows the variation of nominal compressive stress with the volumetric strain. Compressive stress is defined as the reaction force experienced by the hammer divided by the unit cell area and the volumetric strain is calculated by the change in core depth divided by its original value. The core resists buckling until the peak stress point and then the first onset of buckling (Figure 2-5 (a)) starts which causes a sudden drop in the compressive stress. Compressive stress drops until the first folding of the cell wall is complete (Figure 2-5 (b)) and then stress increases. The similar process goes on (though the peaks are very small in comparison to the first peak) until the whole depth of the honeycomb is folded. The crush stress is the average of the oscillatory stress during the cyclic collapse of the foil. Once the entire core is folded, then densification starts resulting very high compressive stress. The crush stress is a vital property which reduces the blast shock transmission by absorbing the energy. Large amount of energy gets dissipated through the plastic deformation of the cell wall at each folding. Higher depth of the honeycomb would produce more folds, thus increase energy absorbing capacity. Although sufficient care has been taken in approximating the load curve, it is not possible to define the crush start and end strain very accurately.

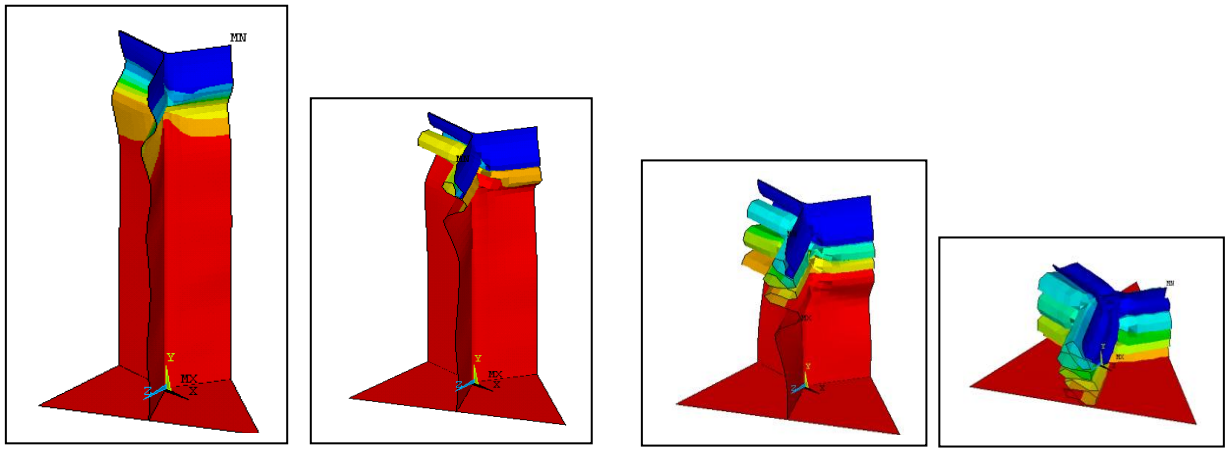

(a) (b) (c) (d)

Figure **2-5**: Different stages of honeycomb unit cell crushing

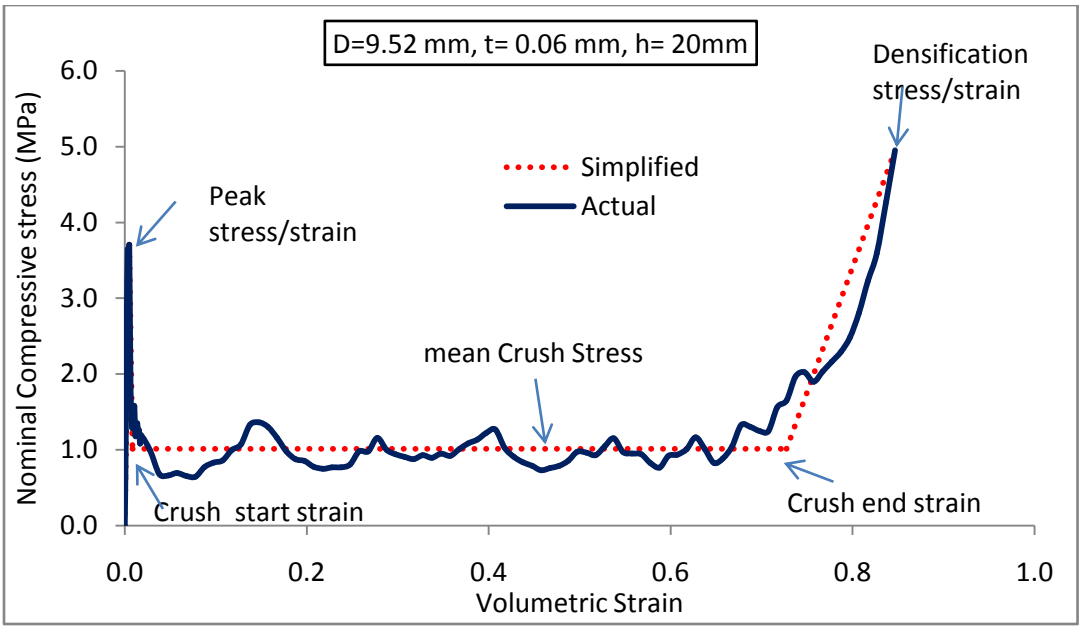

Figure **2-6**: Load curve and its different parameters of the honeycomb core

2.2.1 Mesh convergence study

Three different element sizes (Figure 2-7) are used to study their effect on the load curve. Element size along its depth should be sufficiently small enough to allow the cell wall to fold in a natural way. No noticeable change in load curve is observed when element size is decreased from 0.5mm to 0.25mm.

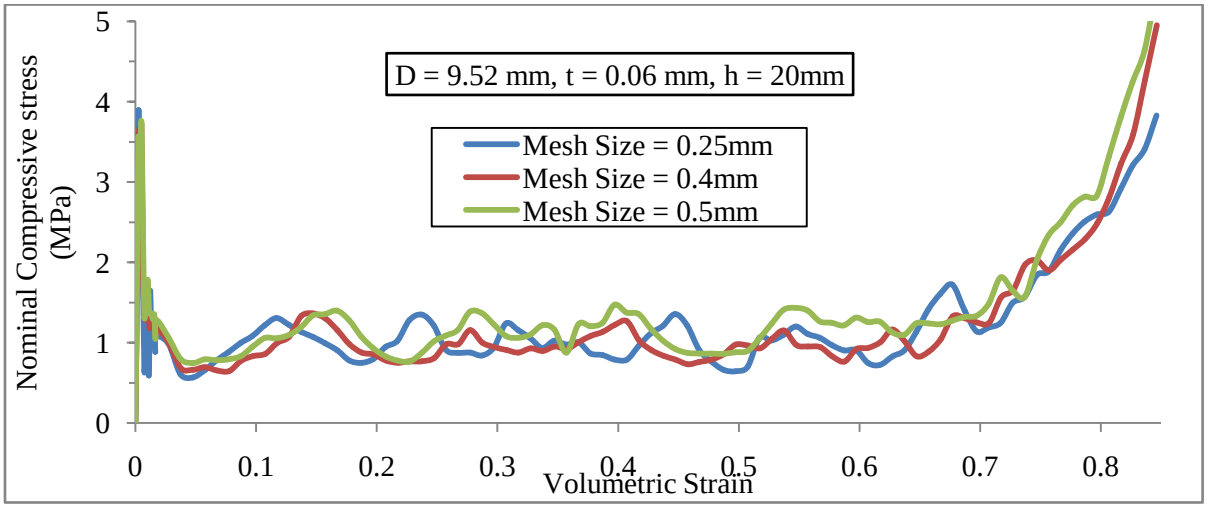

Figure **2-7**: Effect of mesh size on the load curve

2.2.2 Effect of cell dimensions on the folding wavelength

Folding length (2H) refers to the length of the honeycomb along its depth to create a single fold. Folding wavelength (Figure 2-8) is a function of the cell size and the foil thickness (Equation 1-1). It is more sensitive to the cell size than the foil thickness. Precise evaluation of the folding length is vital as it controls the crush strength. Wierzbicki [13] considered that the main constituent of the collapsing cell is the angle element which deforms by developing stationary and moving plastic hinges. Since the strength of the adhesive is smaller than the foil, folding takes place when the two plates adjacent to the bond are partially torn off. For accurate prediction of the crush behavior, the smallest size of the element along the depth of the honeycomb should be smaller than the half of the wavelength (2H). In all the tests, element length of 0.4mm is taken along the honeycomb depth. Figure 2-9 and 2-10 shows the comparison between the wavelengths obtained from the FEA and the analytical equation [13]. The small deviation can be attributed to the end effect and the role of the adhesive strength which aren't considered in the analytical formulation.

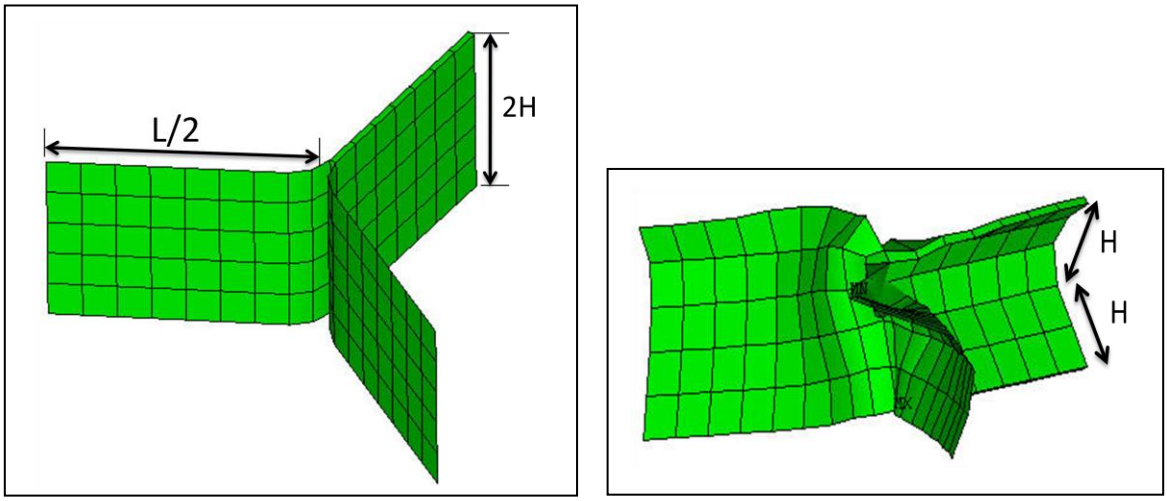

(a) (b)

Figure **2-8**: (a) Typical folding panel and (b) deformation of the folding panel

$$2H = 2 \times 0.821 \times \left[\frac{t \times D^2}{3}\right]^{1/3} \qquad 1\text{-}1$$

$$2H = \frac{Core\ depth}{Number\ of\ foldings} \qquad 1\text{-}2$$

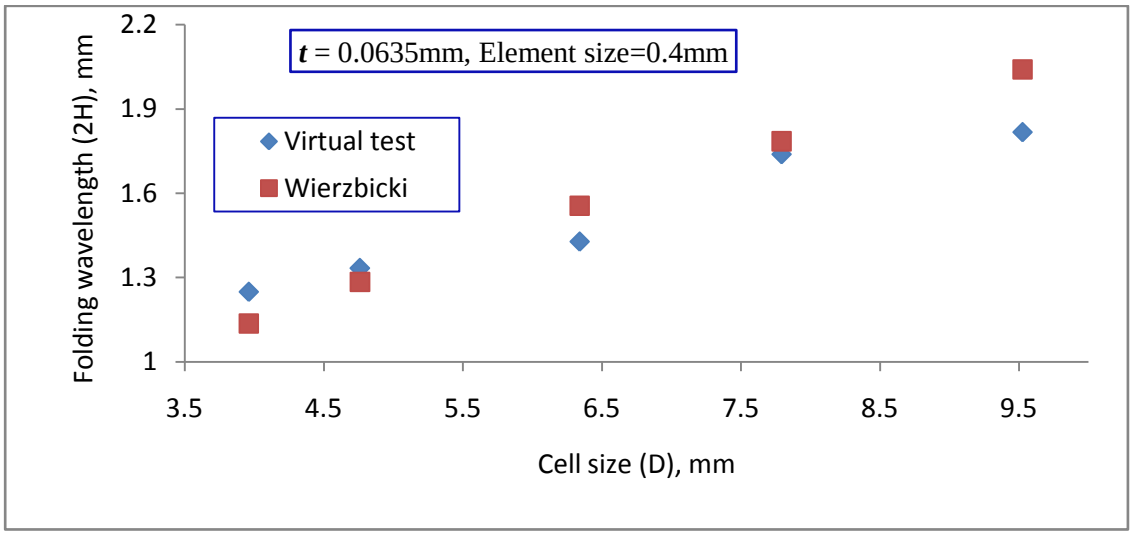

Figure **2-9**: Comparison of the folding wavelength at different cell size

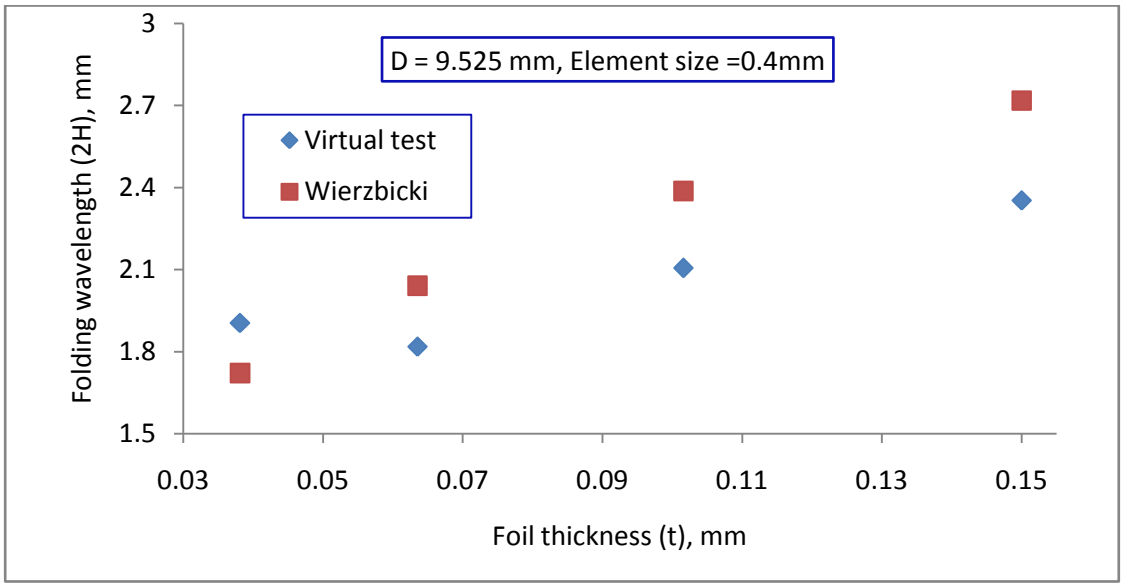

Figure **2-10**: Comparison of the folding wavelength at different foil thickness

2.2.3 Effect of honeycomb cell geometry on the load curve

Following parameters of the honeycomb cell geometry affect its loading curve.

1. Foil thickness, *t*
2. Cell size, *D*
3. Branch angle, *α*
4. Core depth, *h*

Since the regular hexagon cell ($\alpha = 120^0$) gives highest crush strength per unit mass [12], subsequent studies are carried out for the regular cell only. The magnitude of the load curve changes significantly with *D* (Figure 2-11) and *t* (Figure 2-12), but the nature of the curve remain the same. Any change in *D* and *t* alter the mass density of the honeycomb, so load curve is a function of the mass density. Load curve doesn't show any visible change (Figure 2-13) with the core depth. Load curve for *h=5mm* doesn't show any noticeable ripples during crushing. Such a low core depth doesn't allow sufficient number of folds to occur and hence attains densification very fast.

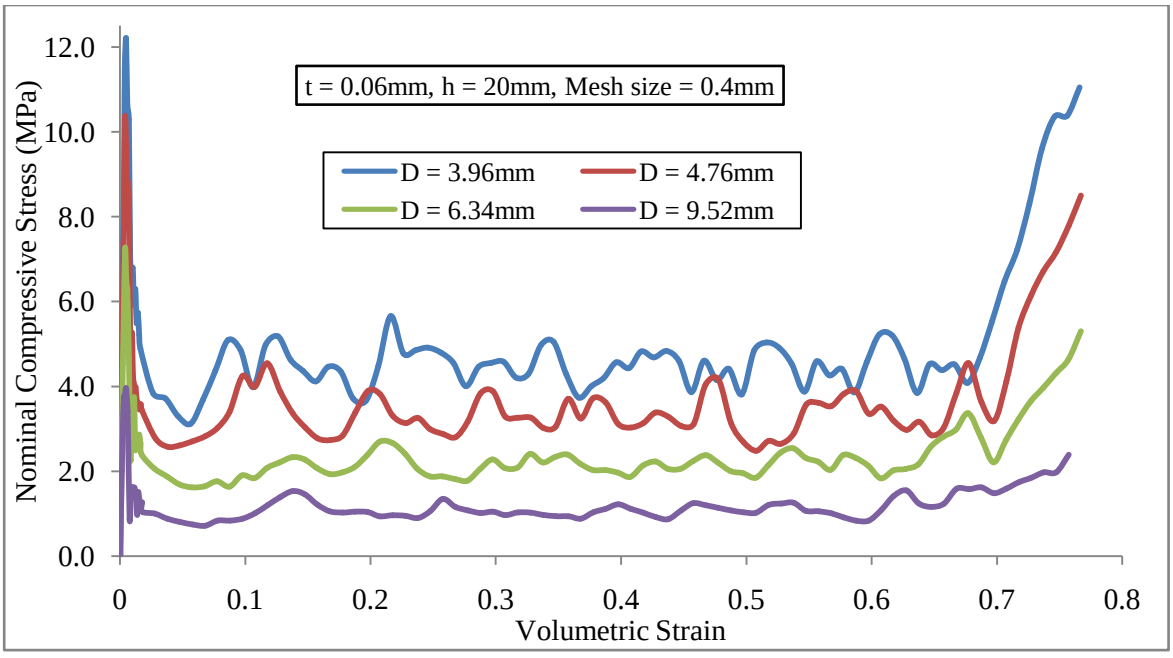

Figure **2-11**: Effect of the cell size *(D)* on the load curve

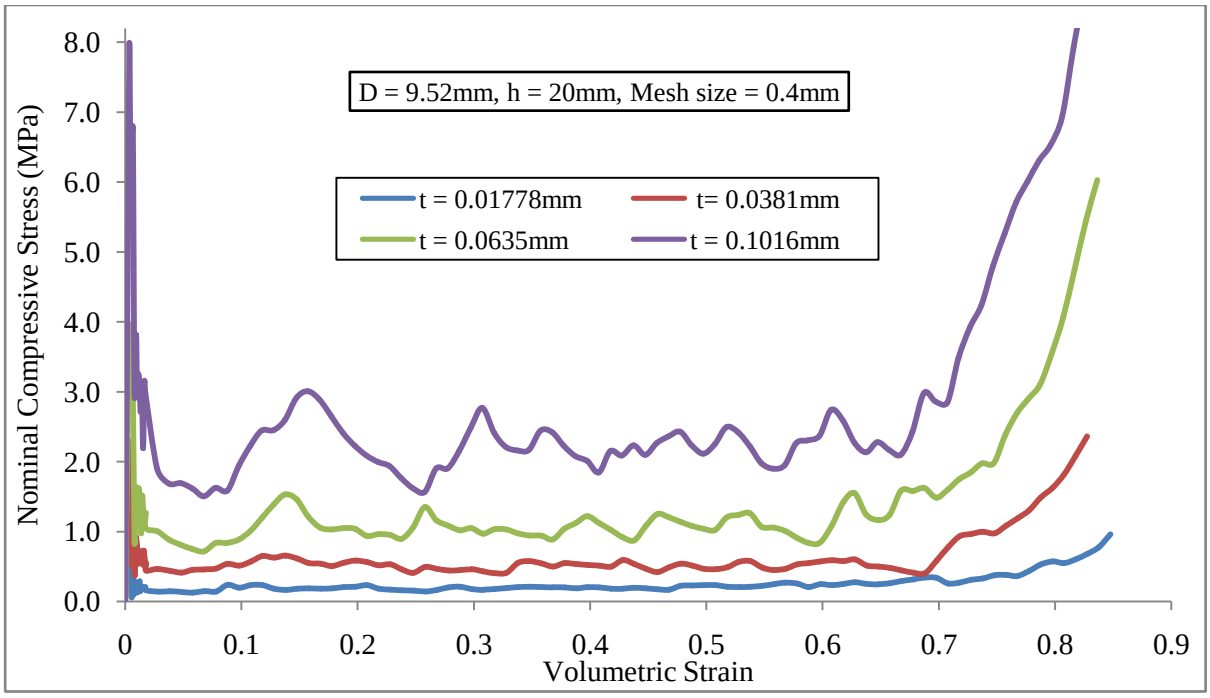

Figure **2-12**: Effect of the foil thickness (t) on the load curve

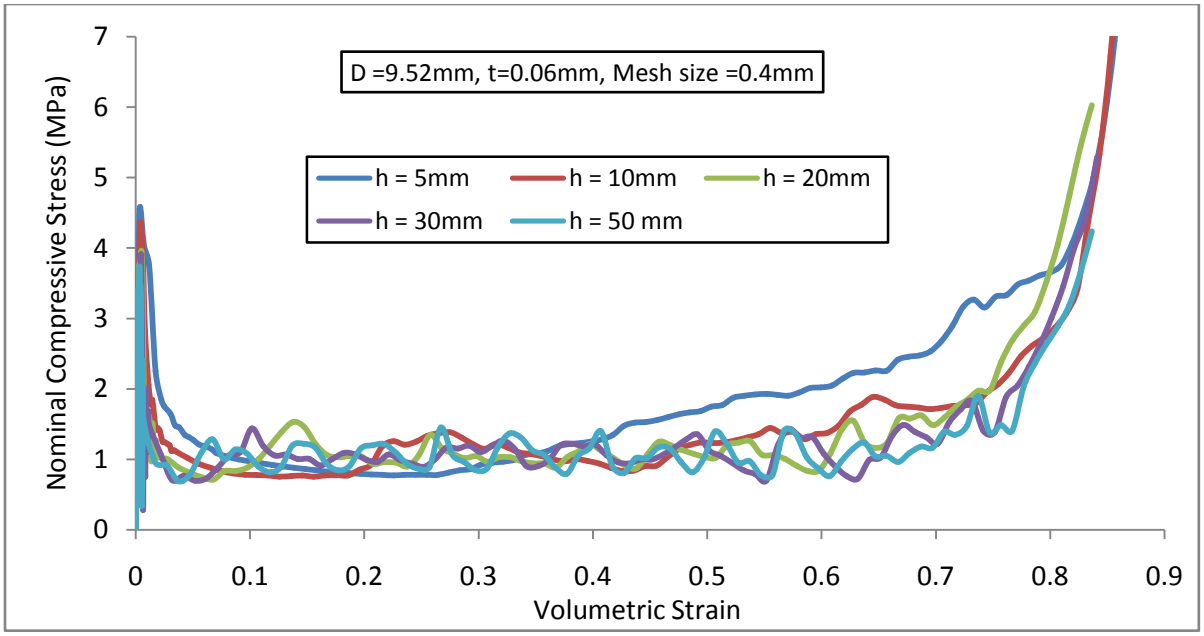

Figure **2-13**: Effect of core depth (*h*) on the load curve

2.3 Parameterization of the load curve in terms of *t* and *D*

2.3.1 Parameterization using response surface method

From above, foil thickness (*t*) and cell size (*D*) govern the load curve. The upper and lower limits of *t* and *D* are defined as per commercially available honeycomb cell sizes [16] for AL5052 material. Central composite design (CCD) method is used to create response equation for the load curve in terms of *t* and *D* using Design-Expert software. Design candidates taken for creating the response equation is shown in Figure 2-14 and Table 2-2. Load curve control points at different design points are mentioned in Table 2-3. Peak stress, crush stress and the densification stress varies considerably with *t* and *D*. Crush start and end strain doesn't show much change with *t* and *D*, hence they can be assumed to be independent. Densification stress is evaluated at strain = 0.85 for all the cases.

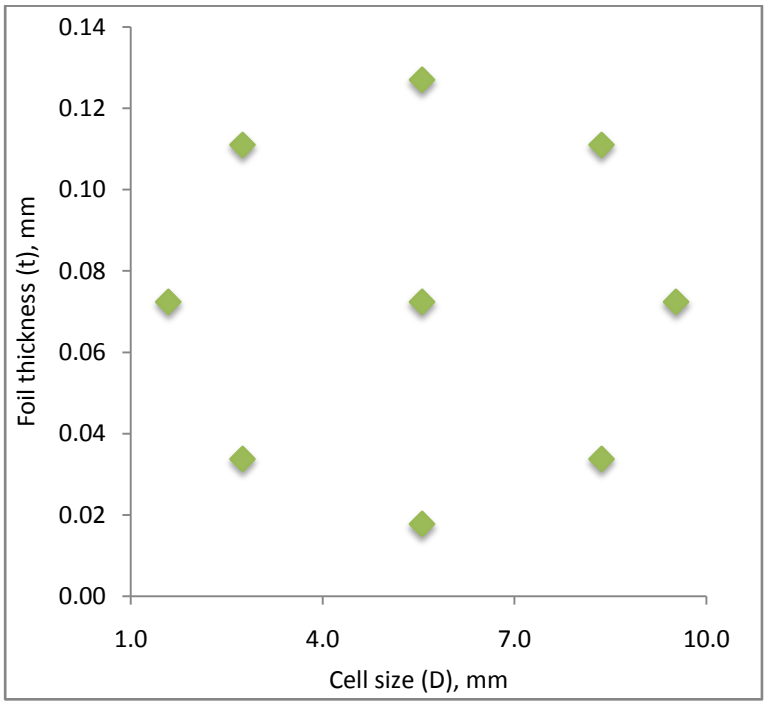

Figure **2-14**: The design candidates for creating response equation using CCD

Table **2-2**: Candidates for creating response equation

Run	Actual factors		Coded factors		Points type
	Cell size (D), mm	Foil thickness (t), mm	Cell size (D)	Foil thickness (t)	
1	5.55629	0.017781	0	-1.414	Axial
2	8.36258	0.111	+1	+1	Factorial
3	5.55629	0.072388	0	0	Center
4	8.36258	0.033775	+1	-1	Factorial
5	2.75	0.033775	-1	-1	Factorial
6	5.55629	0.126994	0	+1.414	Axial
7	1.587597	0.072388	-1.414	0	Axial
8	2.75	0.111	-1	+1	Factorial
9	9.524983	0.072388	+1.414	0	Axial

Table **2-3**: Load curve control points at different design points

Cell Size *(D)*, mm	Foil Thickness *(t), mm*	*t/D*	Peak Stress *(MPa)*	Peak Strain	Crush Stress *(MPa)*	Crush Start Strain	Crush End Strain	Densifi-cation Stress *(MPa)*	Final Strain
9.52	0.072	0.00760	4.97	0.0038	1.42	0.01	0.753	8.13	0.85
5.55	0.127	0.02286	18.6	0.0051	8.2	0.0078	0.752	76.1	0.85
1.58	0.072	0.04560	37.6	0.0074	24.3	0.012	0.745	178	0.85
5.55	0.018	0.00320	1.77	0.0043	0.5	0.0081	0.753	2.76	0.85
5.55	0.072	0.01303	9.63	0.0046	3.5	0.0114	0.723	22.6	0.85
8.36	0.111	0.01327	9.91	0.0039	3.29	0.0086	0.752	23.1	0.85
2.75	0.111	0.04037	33.2	0.0047	19.9	0.011	0.741	182	0.85
2.75	0.034	0.01228	9.99	0.0043	3.48	0.008	0.732	15.9	0.85
8.36	0.034	0.00404	2.93	0.0034	0.6	0.0073	0.744	3.1	0.85

The responses for peak strength crush strength and densification strength determined at design candidate points are used in regression fitting in Design-Expert software. The best response equations in terms of the actual factors are shown below.

$$\log_{10} Crush\ stress = 0.60859 - 0.30062D + 22.16382t - 0.0467Dt + 0.014177D^2 - 79.67109t^2$$

(R^2=0.9895) 1-3

$$\log_{10} Peak\ stress = 0.96878 - 0.22826D + 17.71809t + 0.017612Dt + 0.011204D^2 - 67.25904t^2$$

(R^2=0.9530) 1-4

$$\log_{10} Densification\ stress = 1.14551 - 0.2699D + 25.60747t - 0.42687Dt + 0.013026D^2 - 71.73044t^2$$

(R^2=0.9890) 1-5

2.3.2 Parameterization using *t/D* as a single variable

Wierzbicki [13] showed that the mean crush strength (Equation 1-6) of the metal honeycomb is a function of *t/D*. It is also obvious from the Table 2-3 that peak strength, crush strength and the finals strength are proportional to *t/D*. Figure 2-15, 16 and 17 shows the plot of peak strength, mean crush strength, final strength and peak strain. Their corresponding trend-line is also shown in the plot. Trend line for the peak strength and mean crush strength is well fitted around the virtual testing response data. Trend line for the peak strain is assumed to be linear. Crush start and end strain are assumed to be independent of *t/D* and corresponding strain values are taken as 0.009 and 0.744 respectively. Final strain is fixed at 0.85. Crush strength obtained from the virtual testing matched well (Figure 2-18) with analytical formula developed by Wierzbicki.

$$Crush\ strength = 16.56 \times yield\ strength \times \left(\frac{t}{D}\right)^{5/3}$$ 1-6

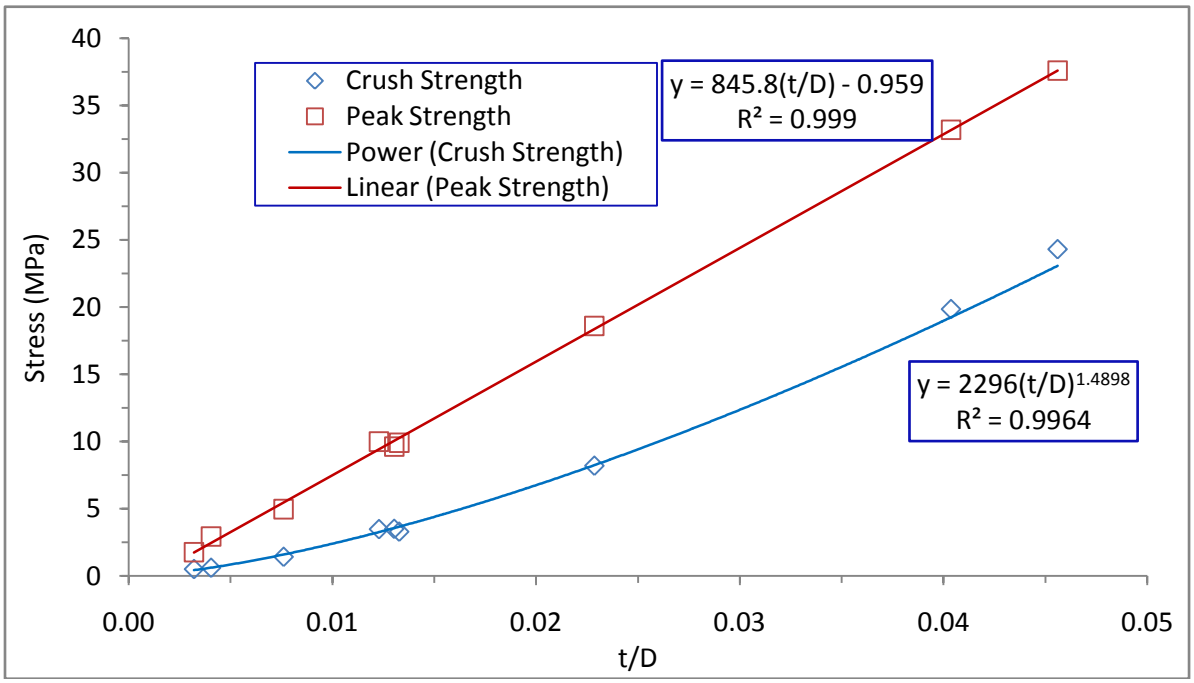

Figure **2-15**: Variation of crush strength and peak strength with *t/D* (Virtual test data and trend lines are shown)

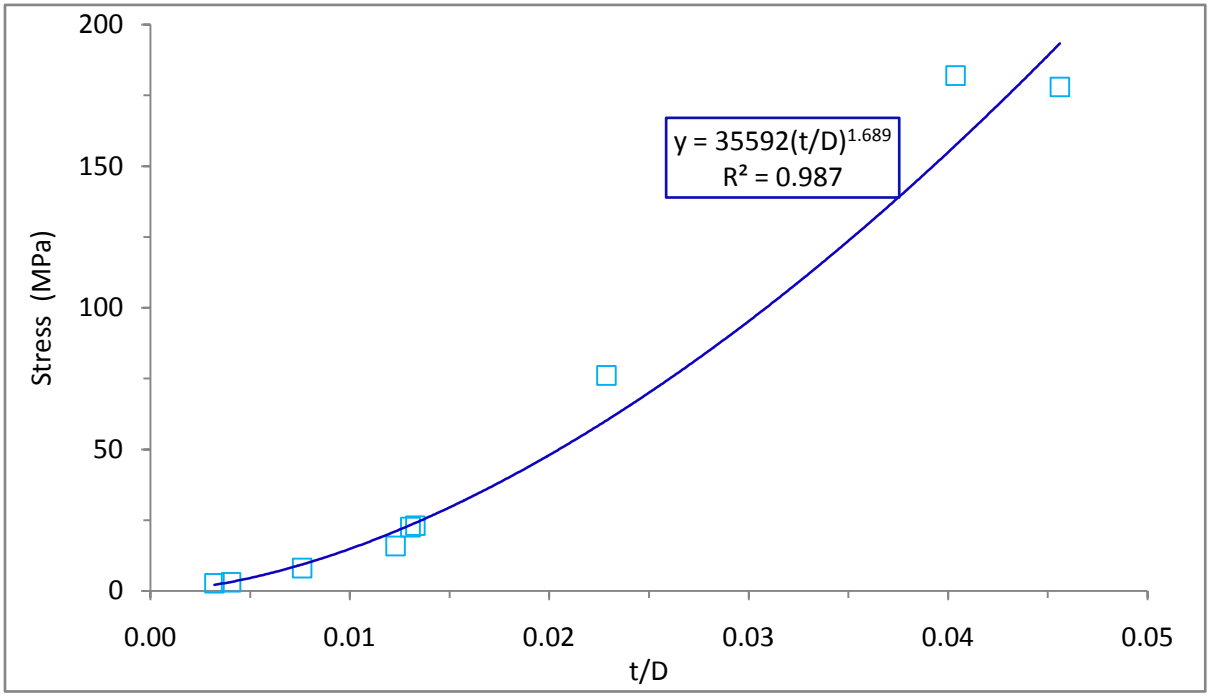

Figure **2-16**: Variation of the densification stress (at strain = 0.85) with *t/D*

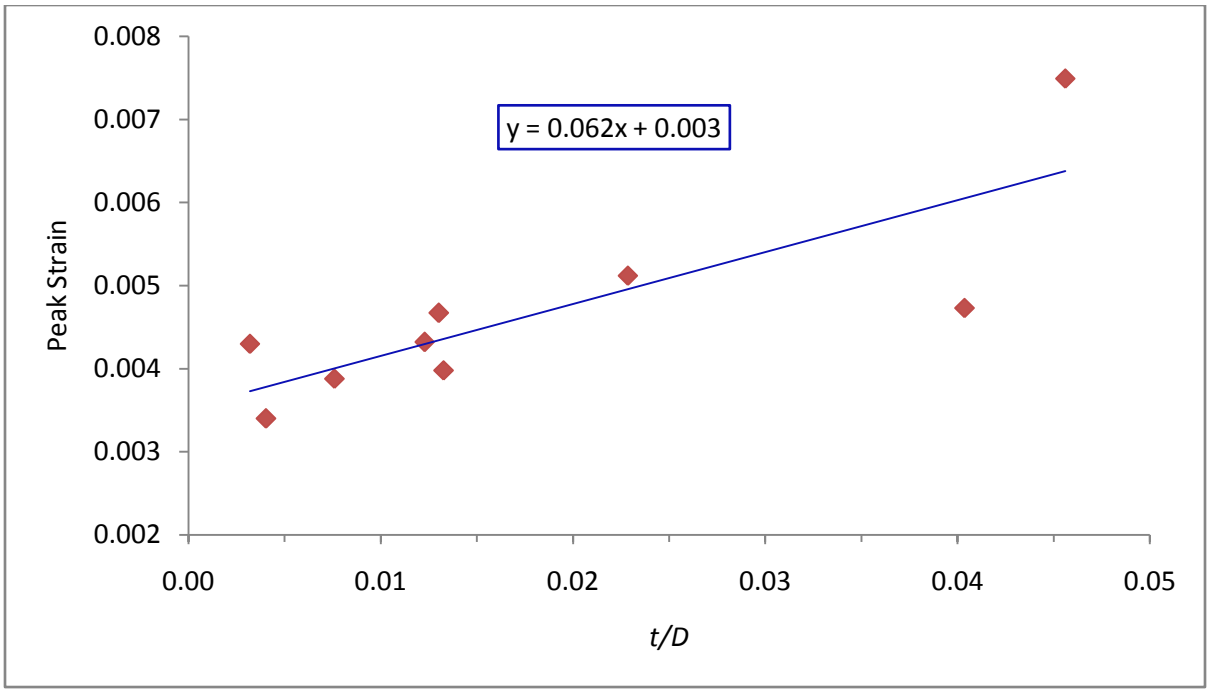

Figure **2-17**: Variation of the peak strain with *t/D*

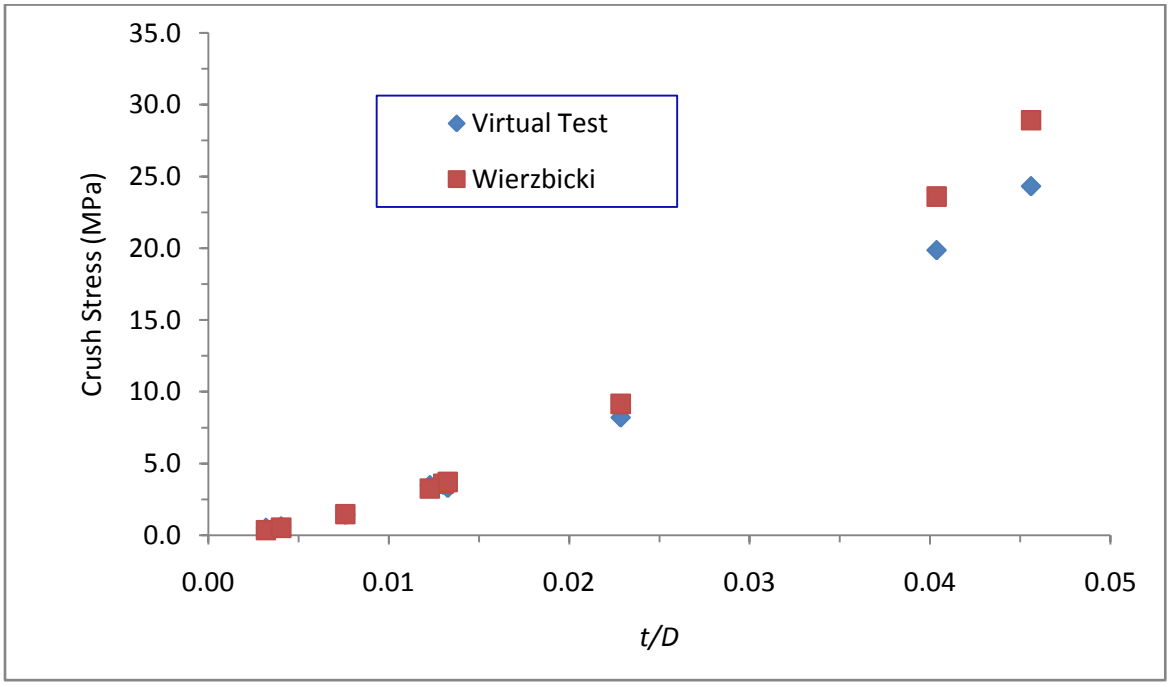

Figure **2-18**: Validation of the crush strength obtained from the virtual test with $Crush\ strength = 16.56 \times yield\ strength \times \left(\frac{t}{D}\right)^{5/3}$ [13]

Crush strength is the most important properties of the load curve. Since it is well represented in terms of *t/D* and handling a single variable in optimization code is easy, the load curve is parameterized in terms of *t/D*. All the relevant parameters used in defining the load curve are given below.

$$Peak\ strain = 0.0626\,(t/D) + 0.0035$$

$$Peak\ stress\ (MPa) = 845.8\,(t/D) - 0.959$$

$$Crushing\ start\ strain = 0.009$$

$$Crushing\ end\ strain = 0.744$$

$$Mean\ Crush\ strength\ (MPa) = 2296\ (t/D)^{1.49}$$

$$Densification\ strain = 0.85$$

$$Densification\ Stress\ (MPa) = 35592\,(t/D)^{1.69}$$

$$Tensile\ stress\ cut\ off\ (MPa) = (8/3)\ \text{Yield stress}\,(t/D)$$

$$Mass\ Density\ (kg/m3) = (8/3)\text{density}\,(t/D)$$

Mass density refers to the mass per unit cell area and per unit depth. Yield stress and density refer to that of AL5052 material.

Chapter-3

Problem Description

3.1 Overview of the problem

Optimal design of a square honeycomb core sandwich panel subjected to air blast loading is considered. Design variables are thickness and shape of the face plates, core depth and core cell size, specifically *t/D* ratio. The objective of the design is to minimize the maximum displacement and subsequently rigid body acceleration of the face plate opposite to the blast, subject to mass and plastic strain limits. These objectives are considered in separate cases. A schematic diagram of the honeycomb sandwich used for optimization is shown in Figure 3-1. The standoff distance of the blast charge is taken as 0.4064 m. A stiffener is used to support the sandwich and to impart sufficient inertia.

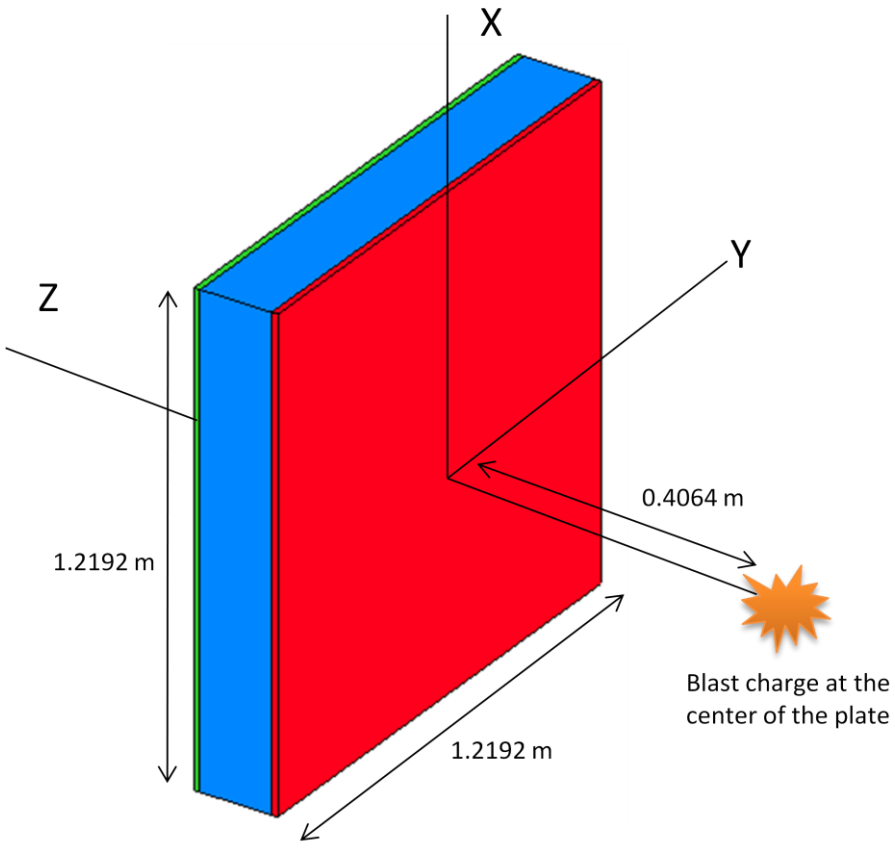

Figure **3-1**: Schematic model of the honeycomb sandwich panel used for optimization

3.2 Honeycomb core sandwich

It is a three layered structure with two face plates and a honeycomb core (Figure 3-2). Front (i.e. charge side) and back face plates are glued to the honeycomb core to make the laminate. The role of face plates is to offer bending stiffness, and the core is meant to absorb energy by crushing and also to enhance bending stiffness of the face plates by maintaining spacing between them. Depending upon the application, different material combination of face plate and core can be used. Metal face plates with high failure plastic strain are preferable. In many structural applications, steel face plates with aluminum core has been used. In our study, aluminum Al5052 is considered for the whole sandwich such that results can be easily compared with Al5052 solid plate.

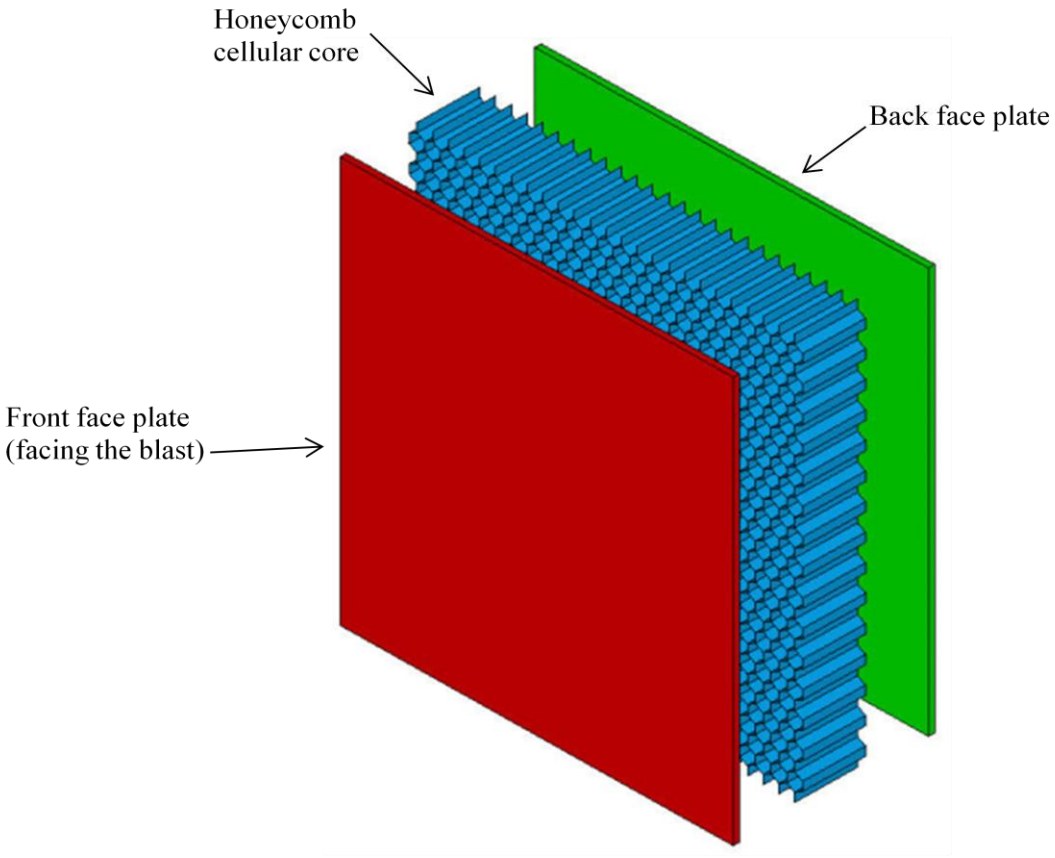

Figure **3-2**: Exploded view of the honeycomb cellular core sandwich panel

3.3 Blast injury

Blast injuries are caused by (I) significant indentations in back face plate, (II) material failure leading to projectile or shrapnel penetration, and (III) high traumatized g-loads which can load the lower parts of the body and create secondary projectiles in the cabin. Thus, minimizing deflection and acceleration of the protective layer (i.e. back face plate in this thesis) while maintaining the structural integrity would mitigate the blast related injuries.

3.4 Problem definition

Mathematically, the design optimization problem can be stated as follows:

Minimize $max\ \delta_b$ (case-1) 3-1

$max\ a_b$ (case-2) 3-2

subject to

$\varepsilon_{pj} \leq \varepsilon_{pmax}$ for each element j of the face plates

$M \leq M_{max}$

$\mathbf{x}^{\mathrm{L}} \leq \mathbf{x} \leq \mathbf{x}^{\mathrm{U}}$

$det\ J_j(\mathbf{x}) \geq 0$ for each element j

Where, the notation is explained in the nomenclature section.

3.4.1 Objective function

The sandwich core is meant as a sacrificing layer and absorbs most of the blast energy, where as front face plate provides sufficient stiffness for better utilization of the core. Back face plate acts as a protective layer for human occupants or cabin equipments. Maximum deflection of the back face plate which characterizes the severity of the blast load is chosen as the objective function to be minimized.

Maximum deflection (same as maximum Z-relative displacement) of the back face plate is shown in the following equation.

$$\delta_b = \delta_{z-max} - \delta_s \quad \text{3-3}$$

Since the sandwich model is not constrained, the maximum Z-deflection of the back face plate is obtained by subtracting the rigid body displacement, specifically, of the stiffener. Displacements along the *x*- and *y*- direction are not significant and are not considered. The displacement is a function of time, and the value at first peak is monitored.

A second objective function is also considered, viz. Z- rigid body acceleration of the back face plate. As this is a function of time, the absolute maximum acceleration is considered.

3.4.2 Constraints

Plastic strain

A plastic strain limit is imposed only on the face plates. No plastic strain limit is imposed on the core. To act as a protective structure, it is very important that the face plates of the sandwich should maintain their structural integrity under the blast loading. The plastic strain of the each element of the face plates increases with simulation time until it reaches a plateau and this saturated or maximum value is considered. The maximum value of the all elements in the face plates is monitored.

Mass constraint

Mass constraint *(M)* considers the mass of the honeycomb core sandwich and the stiffener. Mass of the stiffener remains constant and mass of the sandwich is only evaluated during optimization.

$$M = M_f + M_c + M_b + M_{st} \quad \text{3-4}$$

Design limits

Bounds are imposed on face plate thicknesses and their outward bulge, core depth and *t/D*. Lower limit on the face plate thickness is decided considering the maximum aspect ratio of element as 25. Lower limits on the core depth and *t/D* are taken such as to avoid excessive element distortion. High element distortion stops the simulation on LS-Dyna. Lower limit on the bulge is flat plate i.e. no bulge. Higher limits on the *t/D*, face plate thicknesses, core depth and the bulge are taken such that design space is reasonably sufficient for design space exploration.

3.5 Finite element modeling of the problem

3.5.1 Sandwich model

The model used for this study is shown in Figure 3-3. The model is free to move in space. Back face plate is not restrained and can deform freely without creating high plastic strain. This consideration is very important as the back face plate can transfer the blast load very effectively to the core. The role of the stiffener at the top is to impose high inertia to the back face plate and hence the sandwich. High fictitious density is defined for stiffener. In the absence of the stiffener, the sandwich will fly away without the core getting crushed sufficiently. The core needs the back support from the back face plate to get crushed and that support comes due to presence of the stiffener. The contacts between the face plate and the core, and between the back face plate and the stiffener are defined using *CONTACT features and *TIED_SURFACE_TO_SURFACE_ID card. The tied contact eliminates the separation at the contact face and makes sure that the whole model behaves as a single unit.

Eight noded solid elements are used to mesh all the parts. To consider the bending effect, two layers of element are taken along the thickness of the face plates. Since the core does not offer any bending resistance, a single element layer is taken along its depth. After a mesh convergence study (which is not presented here), 28 X 28 element mesh is taken in x-y plane for the face plates and the core.

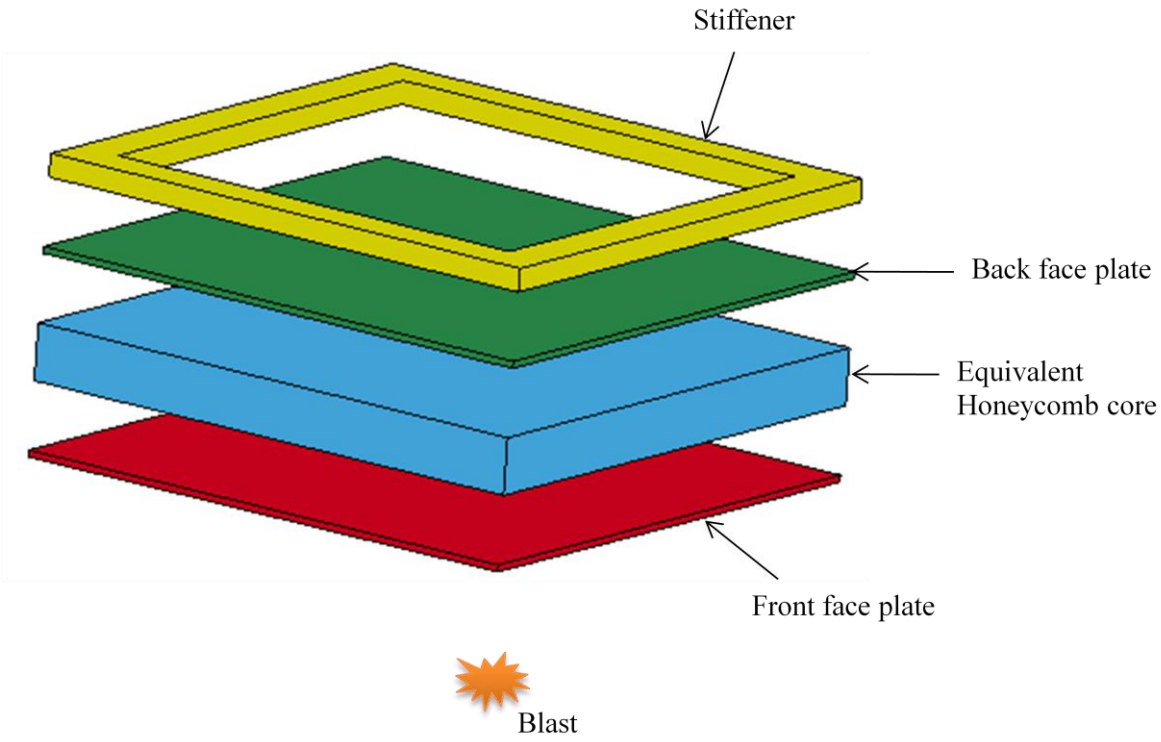

Figure **3-3**: Exploded view of the honeycomb core sandwich model used

3.5.2 Material properties

Aluminum 5052 is used for the face plates. The stiffener also uses the same material but with very high fictitious density i.e. 80180.32 kg/m^3. The *MAT_PLASTIC_KINEMATIC material model is used for them. The honeycomb cellular core is not directly used in the model; however a homogenized solid plate of equivalent mechanical properties to the honeycomb core is used (see chapter-2). The base material for the honeycomb core is also Aluminum 5052. The mechanical property of the core is a function of *t/D* and varies during the optimization process. *MAT_CRUSHABLE_FOAM material model is used for the core. Typical mechanical properties of the core used in this model are shown in Table 3-2 and Figure 3-4. The Poisson's ratio is taken as zero for the core and no damping is considered.

Table **3-1**: Material Properties of Aluminum 5052 used in *MAT_PLASTIC_KINEMATIC input card for the face plates

Property	*Value*
Mass Density	2680 kg/m^3
Young's Modulus	72.0 GPa
Poisson's Ratio	0.34
Yield Stress	300 GPa
Tangent Modulus	50MPa
Hardening Parameter	1.0
Failure Strain	0.038

Table **3-2**: Material Properties of the honeycomb core (for *t/D=0.02677*) made from Aluminum 5052-foil and used in *MAT_CRUSHABLE_FOAM model

Property	*Value*
Mass Density	191.32 kg/m^3
Young's Modulus	4.19 GPa
Poisson's Ratio	0.0
Tensile stress cut off	21.41 MPa
Damping coefficient	0.0

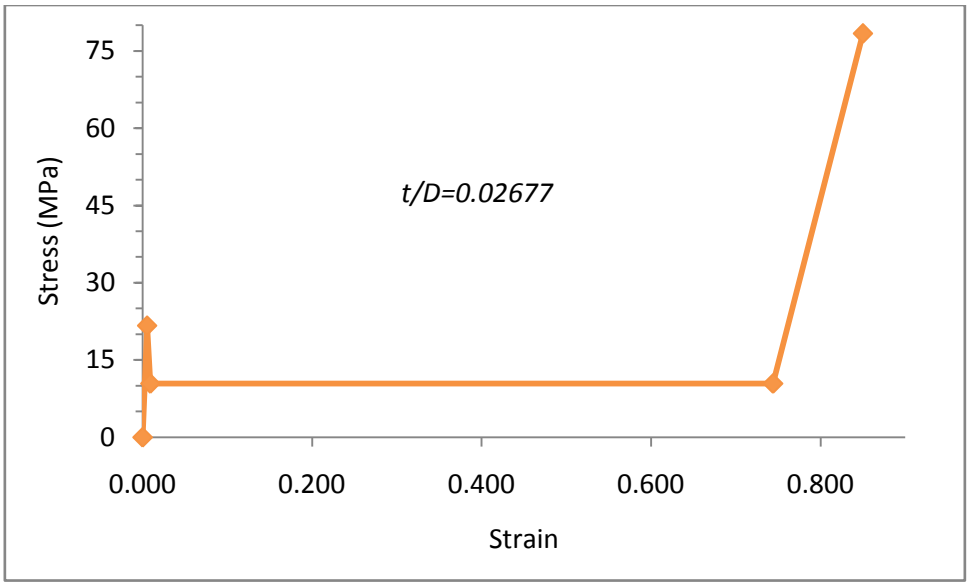

Figure **3-4**: Load curve used in *MAT_CRUSHABLE_FOAM model

3.5.3 Blast load

Blast creates high pressure wave pulses which propagate radially outward from the blast centre until it is stopped by object. The reflected blast wave from the object when meets the incident blast wave creates a single vertical wave front at a certain distance from the object. Any structure between the vertical wave front and the blast source experiences single shock, whereas structure lying above this point experiences a shock history which is resultant of the incident and reflected wave [19]. Blast pressure verses time for a typical blast is shown in Figure 3-5 and is described by Friedlander's Equation 3-5. With time the blast pressure decreases from its peak over pressure value P_0 and goes below the atmospheric pressure at time t_0, then regains to the atmospheric pressure. Since the positive region of the pressure creates damage to the structure, it is only considered for evaluating the blast load. The impulse per unit of the projected area is given in Equation 3-6.

$$P(t) = P_0 \left(1 - \frac{t}{t_0}\right) \exp\left(-\propto \frac{t}{t_0}\right) \qquad 3\text{-}5$$

$$I_s = \int_0^{t_0} P(t)dt = P_0 t_0 \left[\frac{1}{\propto} - \frac{1}{\propto^2}(1 - \exp(-\propto))\right] \quad 3\text{-}6$$

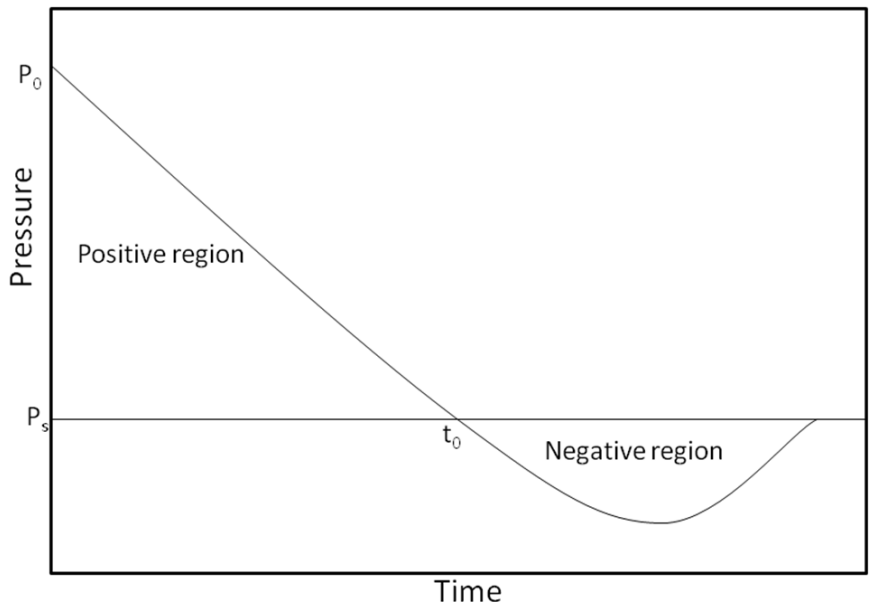

Figure **3-5**: Blast pressure verses time plot

Irrespective of the type of explosive material, the blast load is expressed in terms of equivalent mass of the Tri-Nitro-Toluene (TNT). The blast characteristic of any given mass of the TNT can be obtained from a known blast characteristic of a reference TNT mass using the blast scaling law (Equation 3-7) developed by Hopkinson. No scaling is used on the P_0 and the decay parameter α, but the values correspond to scaled distance and time are used.

$$Z = \frac{R_n}{{W_n}^{1/3}} = \frac{R}{W^{1/3}} \quad 3\text{-}7$$

$$t_{sc} = \frac{t_n}{{W_n}^{1/3}} = \frac{t}{W^{1/3}} \quad 3\text{-}8$$

Ballistic Research Laboratory (BRL) [18] carried out a number of tests using different explosive mass and developed a database in the form of pressure versus radial distance for specified time steps. From the database, BRL derived empirical fit to the data in the form of polynomial functions. It is implemented in CONWEP algorithm which is used in *LOAD_BLAST function of LS-DYNA [20]. Load blast function

uses Friendlander's equation (Equation 3-5) and Hoffman's scaling law (Equation 3-7) to calculate the pressure load for a given TNT amount and standoff distance.

Table **3-3**: Blast load parameters

Parameters	*Value*
Equivalent mass of TNT	8 kg
Blast Location	(0.0,0.0,-0.4064) m
Type of Burst	Air Blast (Spherical Charge)

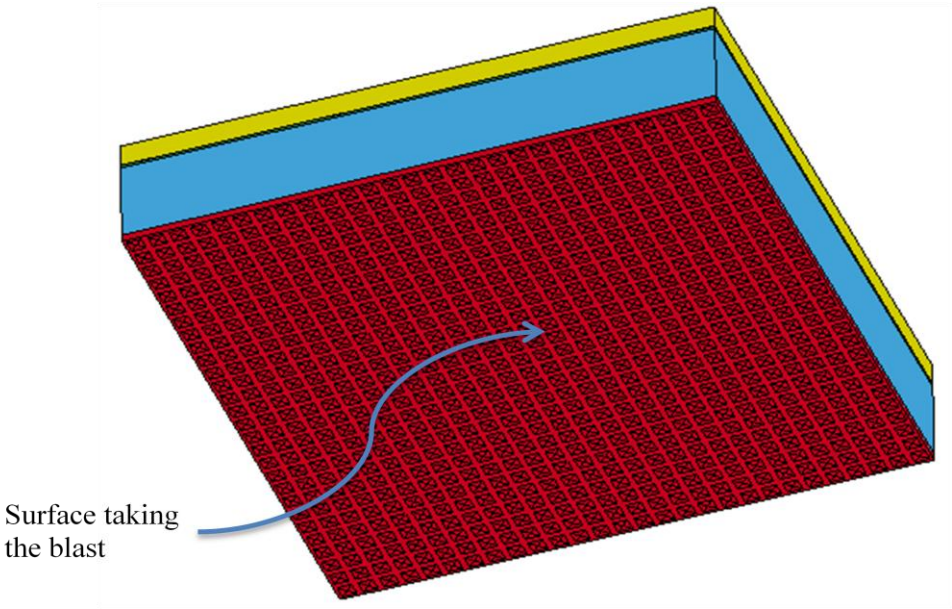

Figure **3-6**: Shows blast surface in the model

The *LOAD_BLAST input parameters (Table 3-3) used are equivalent TNT mass, type of blast (surface or air), load curve, charge location, and surface identification on which blast wave strikes. It ignores the effect of soil type, soil moisture and burial depth of the charge. The blast pressure applied to surface

varies from point to point depending upon the location from blast center and the incidence angle. Higher is the incidence angle, lower is the blast pressure. This is taken care by CONWEP algorithm. The face of the front face plate takes the blast load (Figure 3-6).

3.6 Velocity field for creating the shape (bulge)

A square portion (1.016m x 1.016 m) at the center of the face plates is taken as the domain for applying velocity fields to create the shape. Only convex shapes (outward bulge) are considered. Figure 3-10 shows the sandwich panel with face plates having outward bulges.

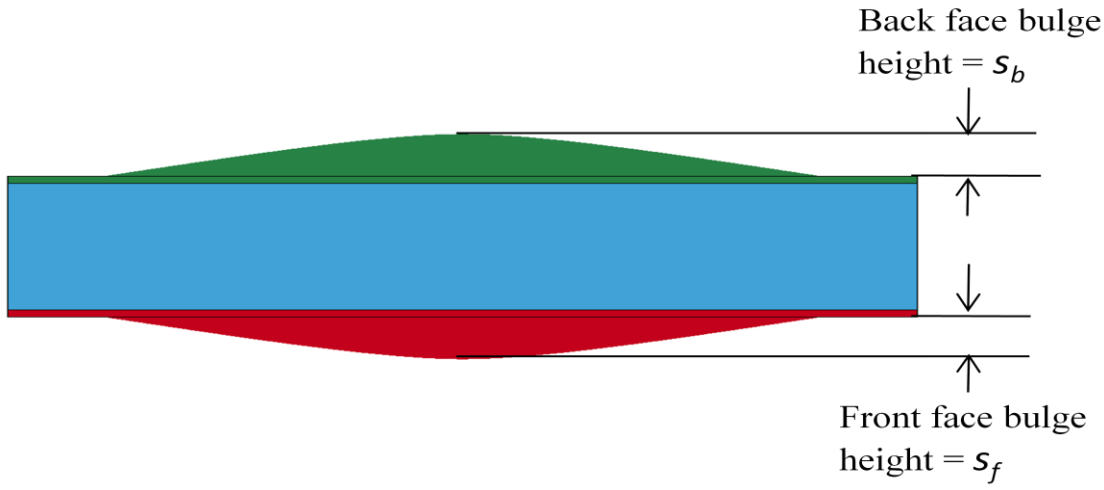

Figure **3-7**: Sandwich panel with permissible bulges at the face plates

The key equations to create and optimize the shape are given in Equation 3-9 and 10.

$$\mathbf{\Delta G} = x_i \mathbf{q}^i \qquad \text{3-9}$$

$$\mathbf{G}(x) = \mathbf{G}_{original} + x_i \mathbf{q}^i \qquad \text{3-10a}$$

and more generally,

$$\mathbf{G}(\mathbf{x}) = \mathbf{G}_{original} + \sum_{i=1}^{N_{dv}} x_i \ \mathbf{q}^i \qquad \text{3-10b}$$

Where **G** is a grid point coordinates vector, representing x-, y-, z- coordinates of all nodes in the model. Each x_k represents the amplitude of a 'permissible shape change vector' or what is commonly called a 'velocity field' or 'basis shape' vector $\mathbf{q}^k$. Vectors $\{\mathbf{q}^k\}$ are generated outside the iterative optimization loop. $\mathbf{G}_{original}$ is the initial shape referred to as the 'baseline' shape. The role of the optimizer is to choose $\mathbf{x}^*$ so that the corresponding shape $\mathbf{G}(\mathbf{x}^*)$ is optimum. As **x** is iteratively changed by the optimizer (DE), the grid point coordinates **G** are updated, an input file is then written and an analysis is carried out to evaluate the various functions in the optimization problem.

3.6.1 Velocity fields

Local point load velocity field is considered which uses the closed form deflection equation for simply supported rectangular plates. This velocity field ensures smooth transition from the flat face to the shape and between basis shapes. $\{\mathbf{q}^k\}$ are generated by determining deformations produced (Equation 3-11) [21] by a fictitious point load *P* at chosen point(s) (η, ξ) (Figure 3-8). Note that other thru-thickness nodes are moved to preserve equal spacing. Each $\mathbf{q}^k$ is normalized.

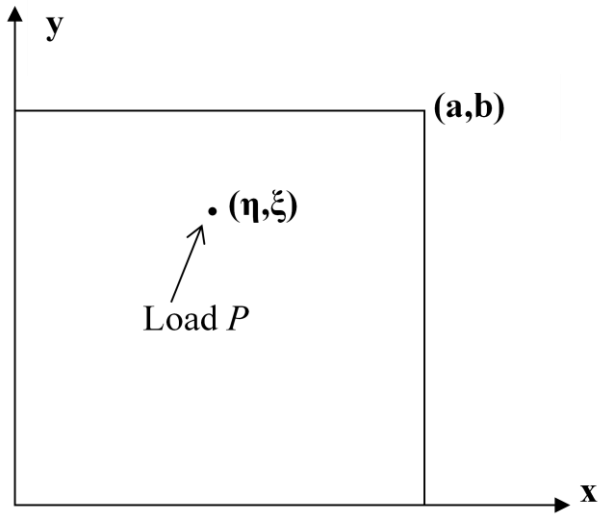

Figure **3-8**: Schematic sketch of rectangular plate

$$W(x,y) = \frac{Pa^2}{\pi^3 D}\sum_{m=1}^{\infty}\left(1 + \beta_m coth\beta_m - \frac{\beta_m y_1}{b}coth\frac{\beta_m y_1}{b}\right.$$

$$\left. - \frac{\beta_m \eta}{b}coth\frac{\beta_m \eta}{b}\right)\frac{sinh\frac{\beta_m \eta}{b}\,sinh\frac{\beta_m y_1}{b}\,sinh\frac{m\pi\xi}{a}\,sinh\frac{m\pi x}{a}}{m^2 sinh\beta_m} \qquad 3-11$$

Where, $\beta_m = \frac{mxb}{a}$, $y_1 = b - y$, $y \geq \eta$

If $y < \eta$, the quantity y_1 must be replaced by y, and the quantity η by $\eta_1 = b\text{-}\eta$ in the above expression.

Five different velocity fields have been generated by considering *P* to be applied, one at a time at (η, ξ) corresponding to four quarter points and one center point, as shown in figures below. These five basis shapes are added (Equation 3-10b) over flat face of the plate to generate the shape (or bulge) as shown in Figure 3-7.

Figures 3-9 to 3-13 show the basis shapes created at five different locations.

Figure **3-9**: Velocity field, $\mathbf{q}^1$ for a point load at the center of the square plate.

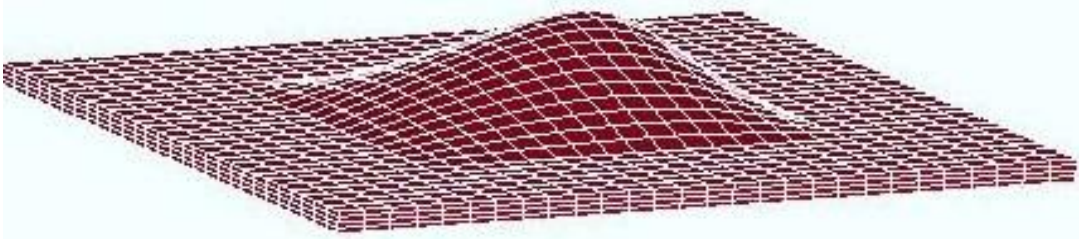

Figure **3-10**: Velocity field, $\mathbf{q}^2$ for a point load at (η, ξ) = (0.75, 0.75) (Note: (η, ξ) for farthest corner is (1, 1)).

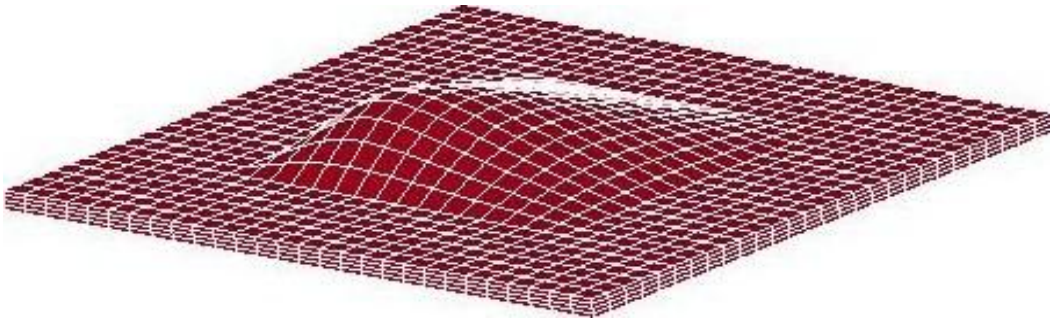

Figure **3-11**: Velocity field, $\mathbf{q}^3$ for a point load at $(\eta, \xi) = (0.25, 0.25)$.

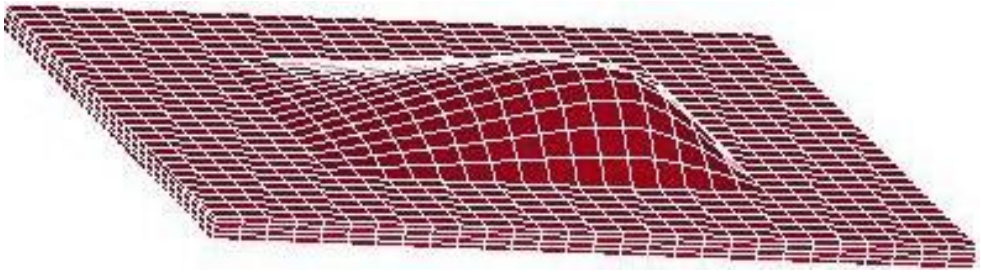

Figure **3-12**: Velocity field, $\mathbf{q}^4$ for a point load at $(\eta, \xi) = (0.75, 0.25)$.

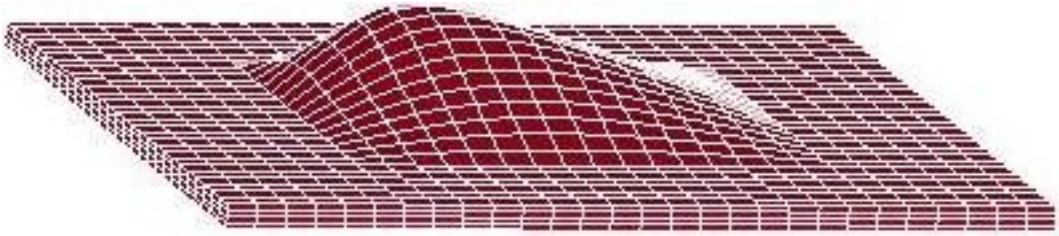

Figure **3-13**: Velocity field, $\mathbf{q}^5$ for a point load at $(\eta, \xi) = (0.25, 0.75)$.

Chapter-4

Size and Shape Optimization

The optimization problem in section 3.4 is carried out in two steps, (I) size optimization, with thickness of the face plates, core depth and *t/D* of the honeycomb core as design variables, and (II) simultaneous size and shape optimization, which includes all the sizing variables as noted above and also the amplitudes of the convex bulges on the both face plates.

Both response surface method (RSM) and differential evolution (DE) technique are used for the optimization. Results from the both methods are compared.

4.1 Overview of the response surface methodology

The main objectives of the Response surface methodology (RSM) are to map a response surface for objective and constraint functions over a particular region of interest and to then optimize. It was introduced by G. E. P. Box and K. B. Wilson in 1951. It uses statistical and mathematical techniques to analyze and optimize the responses influenced by several independent variables [22]. RSM develops response equations by regression fitting to the response data obtained from the designed experiments. Suppose the response y of a system depends upon the controllable input variables $\xi_1, \xi_{2,\ldots,}\xi_k$. The response is expressed as

$$y = f(\xi_1, \xi_2, \ldots, \xi_k) + \varepsilon \qquad 4\text{-}1$$

The true form of the response function *f* is unknown; the above equation represents the approximate form of the response and ε is a statistical error term. The ε is assumed to have normal distribution with mean zero and variance σ^2. The magnitude and standard deviation of the error term can be reduced with suitable selection of the design points and the regression model. RSM uses the coded variables such as $x_1, x_{2,\ldots,}x_k$ which are obtained by transforming the natural variables $\xi_1, \xi_{2,\ldots,}\xi_k$. The coded variables are dimensionless with their mean zero and the same spread or standard deviation.

Different types of regression models such as linear, factorial, quadratic and cubic can be tried to map the response. Each model determines various coefficients of the response equation by minimizing the error. The model which results least minimum error can be accepted as the best model. In most of the cases, linear and quadratic model are proved to be the best. The true response equations in the form of linear and quadratic model in terms of the coded variables $x_1, x_{2,\ldots,}x_k$ are

$$y = \beta_0 + \sum_{i=1}^{k} \beta_i x_i + \varepsilon \qquad 4\text{-}2$$

$$y = \beta_0 + \sum_{i=1}^{k} \beta_i x_i + \sum_{i=1}^{k} \beta_{ii} {x_i}^2 + \sum\sum_{j<i=2}^{k} \beta_{ji} x_j x_i + \varepsilon \qquad 4\text{-}3$$

The coefficients of the equation 4-2 and 4-3 can be determined by least square method i.e. to minimize the sum of square of the error term. The equation 4-2 for *n* number of observations is written in equation 4-4.

$$y_j = \beta_0 + \sum_{i=1}^{k} \beta_i x_{ij} + \varepsilon_j, \; j = 1,2,\ldots.,n \qquad 4\text{-}4$$

The least square function is

$$L = \sum_{j=1}^{n} {\varepsilon_j}^2 = \sum_{j=1}^{n} \left(y_j - \beta_0 + \sum_{i=1}^{k} \beta_i x_{ij} \right)^2 \qquad 4\text{-}5$$

The function *L* is minimized with respect to $\beta_0, \beta_1, \ldots., \beta_k$

$$\frac{\partial L}{\partial \beta_0} = 0 \; and \; \frac{\partial L}{\partial \beta_i} = 0 \,, \; i = 1, 2, \ldots., k \qquad 4\text{-}6$$

Equation 4-4 can be represented in matrix form as

$$y = X\beta + \varepsilon \qquad 4\text{-}7$$

Where,

$$y = \begin{bmatrix} y_1 \\ y_2 \\ . \\ . \\ . \\ y_n \end{bmatrix}, \qquad X = \begin{bmatrix} 1 & x_{11} & x_{12} & \dots\dots & x_{1k} \\ 1 & x_{21} & x_{22} & \dots\dots & x_{2k} \\ & & . & & \\ & & . & & \\ & & . & & \\ 1 & x_{n1} & x_{n2} & \dots\dots & x_{nk} \end{bmatrix}, \qquad \beta = \begin{bmatrix} \beta_0 \\ \beta_1 \\ . \\ . \\ . \\ \beta_n \end{bmatrix}, \qquad \varepsilon = \begin{bmatrix} \varepsilon_1 \\ \varepsilon_2 \\ . \\ . \\ . \\ \varepsilon_n \end{bmatrix}$$

The least square estimate of β which is defined as *b* is given below.

$$b = (X^T X)^{-1} X^T y$$

The covariance matrix of *b* is $Cov(b) = \sigma^2 (X^T X)^{-1}$

Where σ^2 is the variance on *y* and can be defined as

$$\sigma^2 = \frac{SS_E}{n-k-1} \; and \; SS_E = y^T y - b^T X^T y$$

SS_E is the sum of square of the residuals on *y*.

The value of the adjusted coefficient of multiple determinations $R_{adj}{}^2$ is used to judge the quality of the response surface. $R_{adj}{}^2$ is defined as

$$R_{adj}{}^2 = 1 - \frac{SS_E/(n-k-1)}{SS_T/(n-1)} \qquad 4\text{-}8$$

Where $SS_T = y^T y - \frac{\left(\sum_{j=1}^{n} y_j\right)^2}{n}$

The value of the $R_{adj}{}^2$ varies between 0 and 1. Closer its value to 1, better the response surface is.

4.1.1 Central composite design (CCD)

Central composite design method is one of the most commonly used response surface designs for fitting the second order models. This design was introduced by Box and Wilson in 1951. It contains 2^k factorial design points, $2k$ axial design points and $2k$ central design points, where k is number of variables. The factorial points are used to fit all linear interaction points. The axial points are meant for estimating the quadratic terms in the model. Multiple runs at the center of the design space consider the pure error coming from the experiment and also contribute to the estimation of quadratic terms. However in a computational experiment, multiple runs at the same point return same result. Figure 4-2 depicts three types of central composite design for two variable problems depending upon the location of the axial points. The central composite circumscribed (CCC) is the original form of the CCD. The star points define the extreme low and high of the variable and are at α distance from the center. The inner square region defines the design space. These design points have circular, spherical or hyper spherical symmetry. In the central composite face centered (CCF) case, α = ±1. Axial points are at the center of the each face. The central composite inscribed (CCI) is a scaled down CCC design with each factor divided by α. This method is used when the specified design limits are true limits.

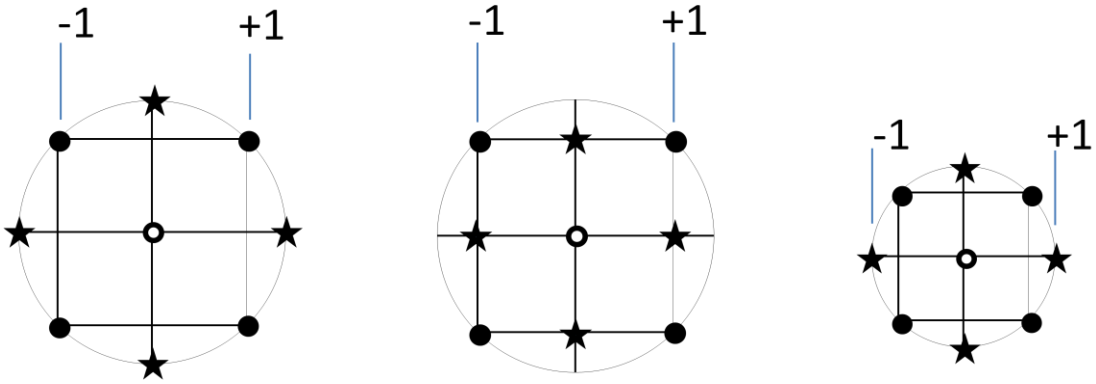

(a) (b) (c)

Figure **4-1**: Three types of CCD designs (a) CCC (b) CCF and (c) CCI

To maintain the rotatability,

$$\alpha = [2^k]^{1/4} \qquad 4\text{-}9$$

Sometimes, depending upon the number of design variables *k*, practical value of α which is less than from the equation [22] can be taken.

4.1.2 D-Optimal design

D-Optimal design is mostly used because of two reasons. First, when the standard factorial design such as CCD requires too many runs (or experiments) for the resources or time available. Second, when it is not feasible to run all the design points in the design space or design space is not rectangular. This design minimizes the covariance $(Cov(b))$ of the parameter estimates for a pre-defined model which is equivalent to maximizing the determinant $D = |X^T X|$. Unlike traditional designs, D-Optimal design does not need to have orthogonal matrices.

4.2 Overview of the Differential Evolution

Differential evolution (DE) is a stochastic parallel direct search evolution strategy (ES) optimization method for finding the global minimum of non-differentiable, nonlinear and multimodal objective functions. This method is fairly fast and reasonably robust. The basic outline of the DE is cited below.

1. [Start] Initial populations of n-chromosomes (potential solutions) are generated randomly. If at all a preliminary solution is available, then initial population can be generated by adding normally distributed random deviations to the nominal solution.

2. [Mutation] New vector is generated by combining the weighted difference of two population vectors with a third vector randomly chosen from the current population.

3. [Crossover] Mutant vector is mixed with a preset target vector to generate trial vector.

4. [Fitness] Evaluate fitness function f(x) for the trial and target vector.

5. [Selection] Whichever (out of trial and target vector) yields a reduction in the value of fitness function is accepted for the next generation.

6. [Test] If the termination criteria (Maximum number of generations or convergence control) are satisfied, then print the best solution.

7. [Loop] Go to step 2.

4.2.1 Mutation

Mutant vectors are generated by the following equation

$$V_{i,G+1} = X_{r_1,G} + F\left(X_{r_2,G} - X_{r_3,G}\right) \qquad 4\text{-}10$$

Where, $X_{i,G}, i = 1, 2, 3 \ldots\ldots NP$ is the population vector for generation G and $V_{i,G+1}$ is the mutant vector for generation G. r_1, r_2 and r_3 are random indices belonging to (1,2,3….NP). F >0 (in between 0 to 2) is the weight factor and controls the amplification of the differential variation. This condition implies that NP must be at least four.

DE is quite different to genetic algorithm (GA)/ES in its perturbation technique. DE uses the difference of two randomly chosen population vector to perturb an existing vector. Where as in GA/ES, predetermined probability distribution functions are used to determine the vector perturbations.

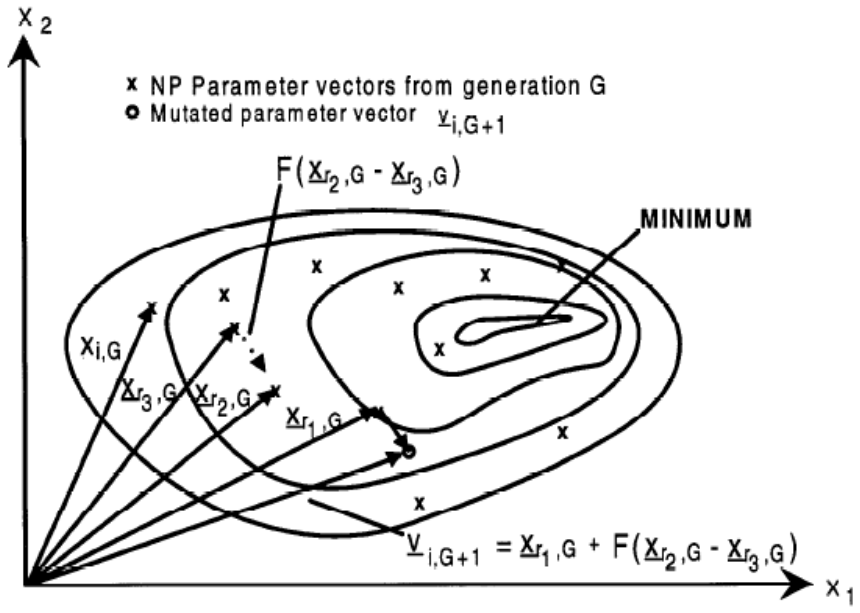

Figure **4-2**: An example for two dimensional cost functions showing the contour lines and generation of mutant vector

4.2.2 Crossover/Recombination

Crossover is applied to the mutant vectors to increase the diversity. The resulting vector is called a trial vector. A trial vector $U_{ji,G+1}$ is a mixture of mutant vector and target vector$X_{ji,G}$. Their degree of mixing depends upon the two conditions as shown in Equation 4-11.

$$U_{ji,G+1} = \begin{cases} V_{ji,G+1}, & If\ (randb(j) \leq CR)\ or\ j = rnbr(i) \\ X_{ji,G}, & If\ (randb(j) > CR)\ or\ j \neq rnbr(i) \end{cases} \qquad 4\text{-}11$$

Where, $j = 1, 2, 3, \ldots\ldots, D$ indicates the parameters in each vector.

$randb(j)$ is the j[th] evaluation of a uniform random number generator with outcome $\in (0,1)$. CR is crossover ratio constant $\in (0,1)$ which is defined by the user. $rnbr(i)$ is a randomly chosen index $\in 1, 2, 3, \ldots\ldots, D$. This logic is so well designed that trial vector gets at least one parameter from the mutant vector.

4.2.3 Selection and generation gap

In the selection, greedy criteria are followed. Whichever out of trial and target vector yields a reduction in the value of fitness function is accepted for the next generation. DE is an overlapping model where parent (target vector) and offspring (trial vector) compete for the population slot for next generation. For each population slot there is equal chance among parent and offspring of getting selected. So it indicates that that DE neither follows elitist strategy nor steady state (generation gap=1) evolution algorithm (EA), whereas GA selects from the global set of off springs and ES from global set of parents and off springs.

4.3 Optimization by response surface method

Design Expert, commercially available software is used for mapping the response surface in the design space. It implements the RSM to develop the response equation. Using the response equations, optimization is carried out by FMINCON, a gradient based optimizer in MATLAB optimization toolbox. Figure 4-3 shows the overview of the steps followed for optimization. Since the lower limit on the factor is the design limit, CCF method is adopted to create design points. It uses only 3 levels for each factor. Figure 4-4 and 4-5 shows the design parameters used. Table 4-1 and 4-2 shows the design factors used in CCD to create response equations.

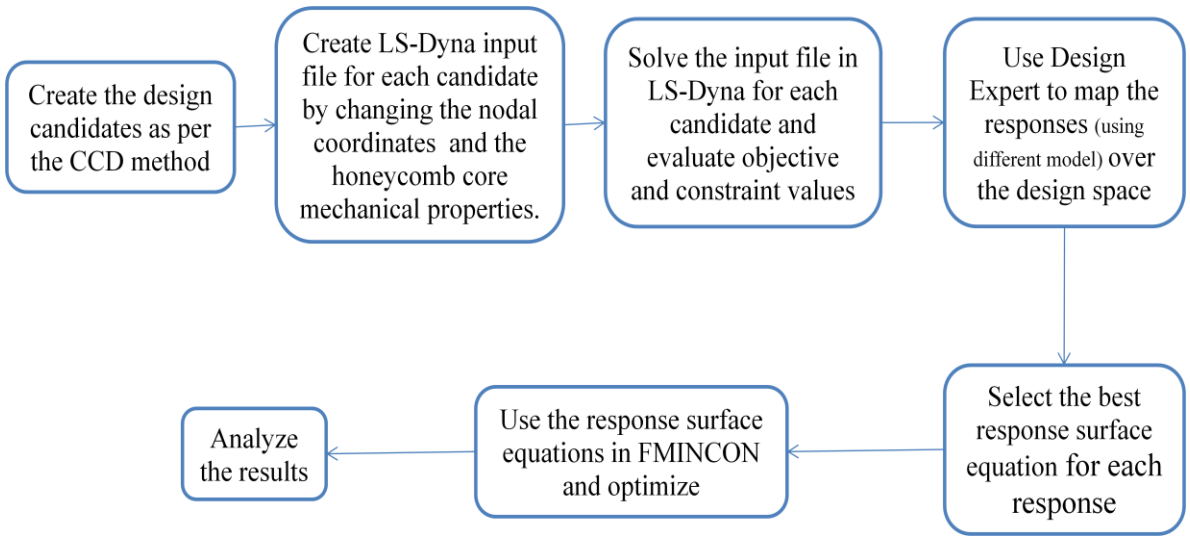

Figure **4-3**: Flow chart of the steps followed for optimization using RSM

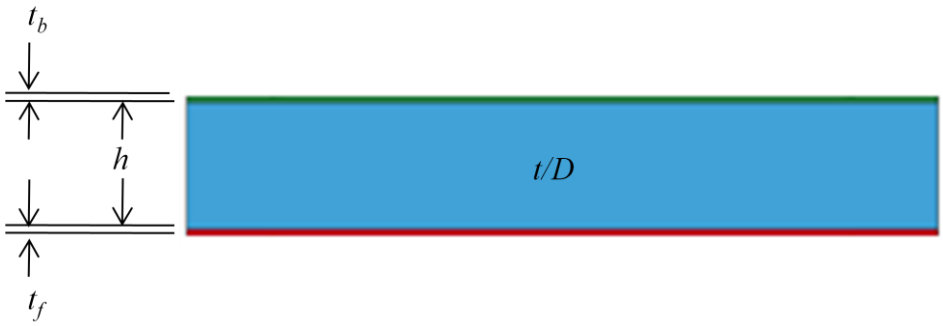

Figure **4-4**: Schematic model showing the size design parameters

Table **4-1**: Actual and coded factors used in CCD for size optimization

Coded factors (α=1)→		*-1 (lower limit)*	*0*	*+1 (upper limit)*	
Front face plate thickness (mm)	t_f	3.5	10.75	18	Actual factors
Core height (mm)	h	200	475	750	
Foil thickness/cell size	t/D	0.00754	0.02677	0.046	
Back face plate thickness (mm)	t_b	3.5	10.75	18	

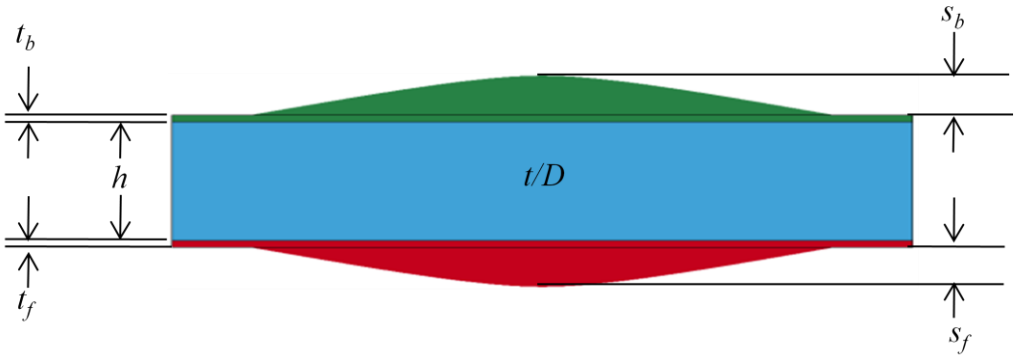

Figure **4-5**: Schematic model showing the size and shape design parameters

Table **4-2**: Actual and coded factors used in CCD for simultaneous size and shape optimization

Coded factors (α = 1) →		*-1(lower limit)*	*0*	*+1(upper limit)*	
Front face plate thickness (mm)	t_f	3.5	10.75	18	Actual factors
Core height (mm)	h_c	200	475	750	
Foil thickness/cell size	*t/D*	0.00754	0.02677	0.046	
Back face plate thickness (mm)	t_b	3.5	10.75	18	
Front face plate bulge (mm)	s_f	0	50	100	
Back face plate bulge (mm)	s_b	0	50	100	

Sizing optimization has four design variables (*k=4*) and number of design candidates required for CCD is determined by following equation.

$$N = 2^k(factorial\ points) + 2k(axial\ points) + 2k(center\ points) =$$
$$16 + 8 + 1(no\ repetition) = 25 \qquad 4\text{-}12$$

2k at the center point refers to the *2k* experiments for a single design candidate. Since computational experiment produces same result, only one run is considered. Similarly for sizing and shape optimization (*k=6*), the number of design candidates required for CCD is 77.

4.3.1 Responses for size optimization

In most cases quadratic polynomial fit gives better fit. The responses are mapped in the design space by using different types of transformation functions. The best response equations are selected after evaluating its R_{adj}^2 value and standard deviation. The response surfaces of displacement (δ_b) and acceleration (a_b) for a typical case obtained for size optimization (k=4) is given in Figure 4-5. No response for the mass is fitted as an analytical formula exists.

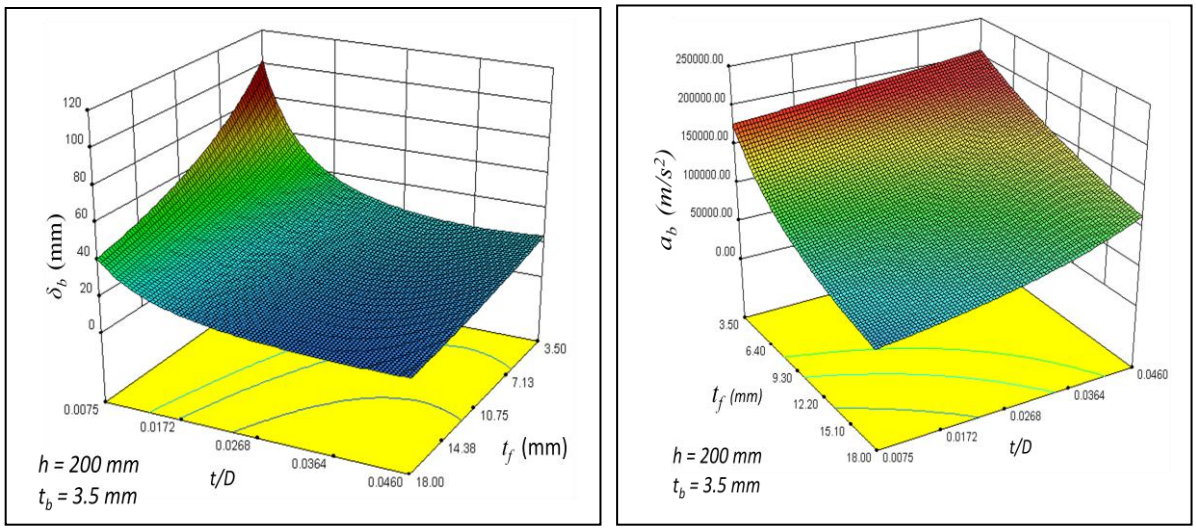

(a) (b)

Figure **4-6**: Response surface for (a) maximum back face *Z*-relative displacement and (b) *Z*-rigid acceleration of back face plate

4.3.2 Responses for size and shape optimization

In a similar fashion, the responses are mapped and the best response equations are selected. Since shapes are involved here, response equation for the mass is developed instead of building its complex analytical form. The response surfaces of displacement (δ_b) for simultaneous size and shape optimization (k=6) are given in Figure 4-6. No size and shape optimization is carried out for minimizing a_b.

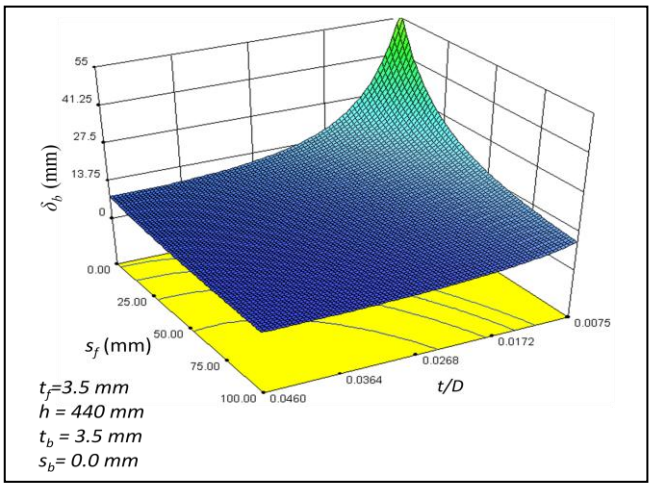

Figure **4-7**: Response surface for maximum back face Z-relative displacement of back face plate

4.4 Optimization by Differential Evolution

The optimization code implementing DE algorithm developed by Vikas et al [1] for shape optimization of solid plate subjected to blast loading is used here. This code is modified to handle the present honeycomb core sandwich model. For every design evaluation, the code updates the geometry of the model and the material properties of the honeycomb core. Since the function evaluations of a population of design can be done independently, parallel processors in a cluster are used to speed up the optimization process. Figure 4-7 describes the overall steps followed for the optimization. The same design limits are used as in case of RSM with FMINCON. Generation limit is considered as termination criteria. The best deign value out of 30 generation evaluations is considered as the optimum. Table 4-3 shows the input parameters used in the optimization. Optimization using DE is only carried out to minimize δ_b.

Table **4-3**: Typical values of input parameters used in the input file

Parameter	*Value*
Generation limit	30
Population size	50
Mass of the assembly (kg)	2000-2100 kg
Plastic strain limit	0.038

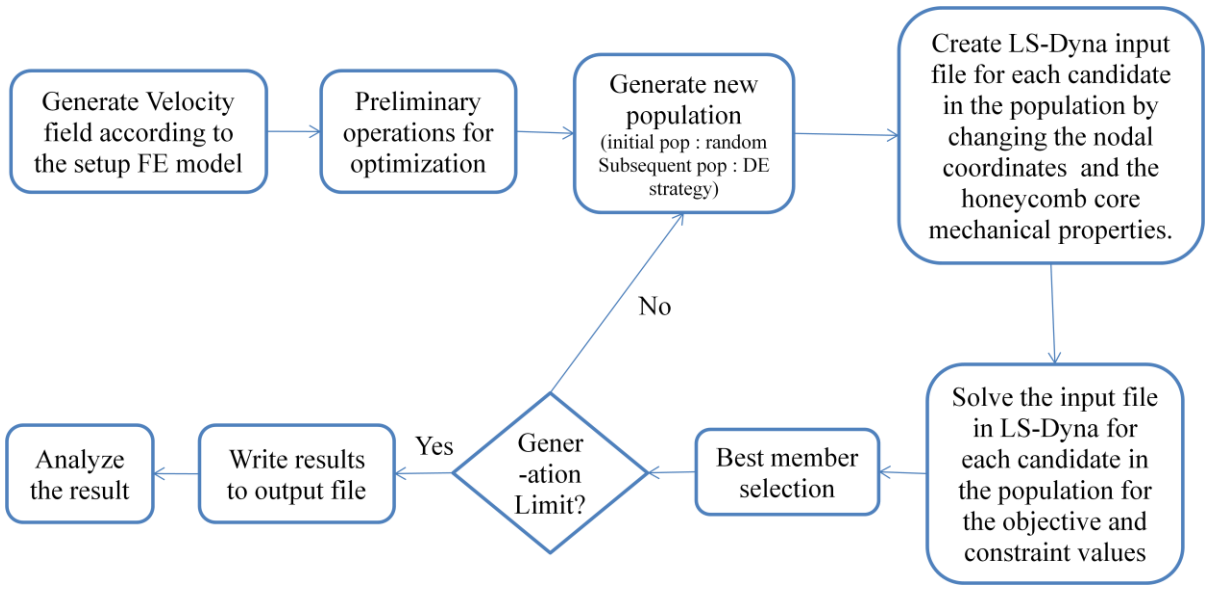

Figure **4-8**: Flow chart of the steps followed for optimization using Differential Evolution

4.5 Relative ease of using RSM and DE for optimization

Once the response equations are obtained from the RSM, then it is very easy to use FMINCON for optimization. Since FMINCON is based upon gradient method, optimization process is very fast and accurate. The overall accuracy of the result depends upon the quality of the response surface fit. Optimization using DE is time consuming since it evaluates a large number of function evaluations. For 50 population size and 30 generations, 1502 number of function evaluations is required. A single optimization process takes ~20hr in LION-XC cluster which has 8 processors (one master and 7 slaves). Each processor is of dual 3.0-GHz Intel Xeon 3160 (Woodcrest) Dual-Core Processors with 16 GB of ECC RAM. DE is expected to produce more accurate result than RSM-FMINCON.

Detailed optimization study is carried out using RSM and the results are compared with DE results for $\boldsymbol{\delta_b}$ only at some selected mass of the sandwich.

Chapter-5

Numerical Results

5.1 Introduction

Optimization is carried out at different mass limits of the sandwich. Detailed results are presented for 150 kg mass limit of the sandwich. Nomenclature used here is given in Table 5-1 and design bound given in Table 5-2. The optimization study is carried out for a fixed amount of charge, viz. 8 kg TNT. The effective blast load on the structure varies with the shape of the front face as well as the magnitude of the dishing deformation of the front face plate (Figure 5-1). Considering blast in air, a convex bulge reduces the effective blast load by deflecting the blast wave outward, while a concave shape increases the impulse imparted to the structure resulting in increased effective blast load. Further, a dishing deformation in a flat panel also increases the effective blast load. This effective blast load is discussed in terms of the magnitude of the saturated Z-momentum of the whole structure, which equals the saturated Z-impulse imparted to it. The δ_b, a_b, ε_{pmax} and total *Z*-impulse values given in this Chapter refer to the LS-DYNA output.

Table **5-1**: Nomenclature used in optimization

Front face plate thickness (mm)	t_f
Core height (mm)	h
Foil thickness/cell size	t/D
Back face plate thickness (mm)	t_b
Front face plate bulge height (mm)	s_f
Back face plate bulge height (mm)	s_b
Back face plate maximum relative displacement in *Z*-direction (mm)	δ_b
Back face plate maximum rigid body acceleration in *Z*-direction (m/s^2)	a_b
Sandwich mass (kg)	M

Table **5-2**: Bounds on design variables

	Lower bound	Upper bound
t_f (mm)	4.4	18
h (mm)	200	750
t/D	0.00754	0.046
t_b (mm)	4.4	18
s_f (mm)	0	100
s_b (mm)	0	100

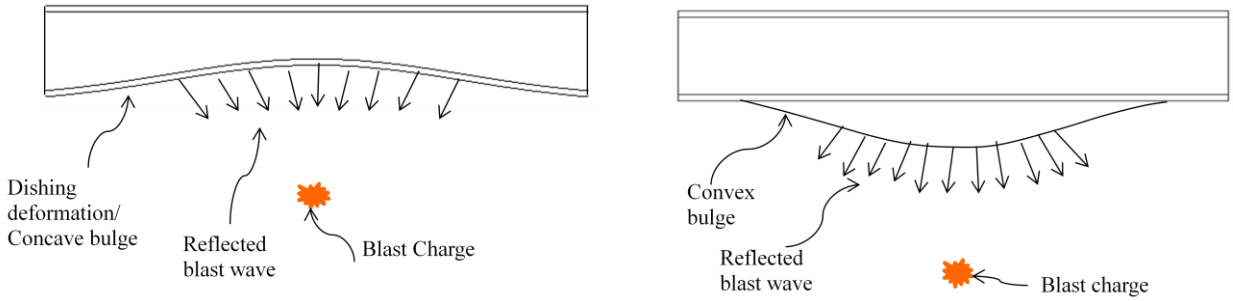

(a) (b)

Figure **5-1**: Reflection of blast wave from (a) concave bulge and (b) convex bulge at front face plate

5.2 Optimization results for minimum displacement, δ_b

Figure 5-2 shows the optimized sandwich panel for 150 kg mass and compares the optimized results with same mass solid plate. Size optimized sandwich panel results in 72.44% reduction in δ_b from a uniformly thick solid (i.e. homogeneous) plate of equal mass. Such a high percentage reduction in δ_b indicates that the sandwich structure can be effectively used to mitigate the effects of blast loading. Comparison of the honeycomb sandwich with a shape-optimized solid metal plate is given later in this Chapter. Further reduction by 15.1% in δ_b can be achieved by simultaneous size and shape optimization of the sandwich structure (Figure 5.2).

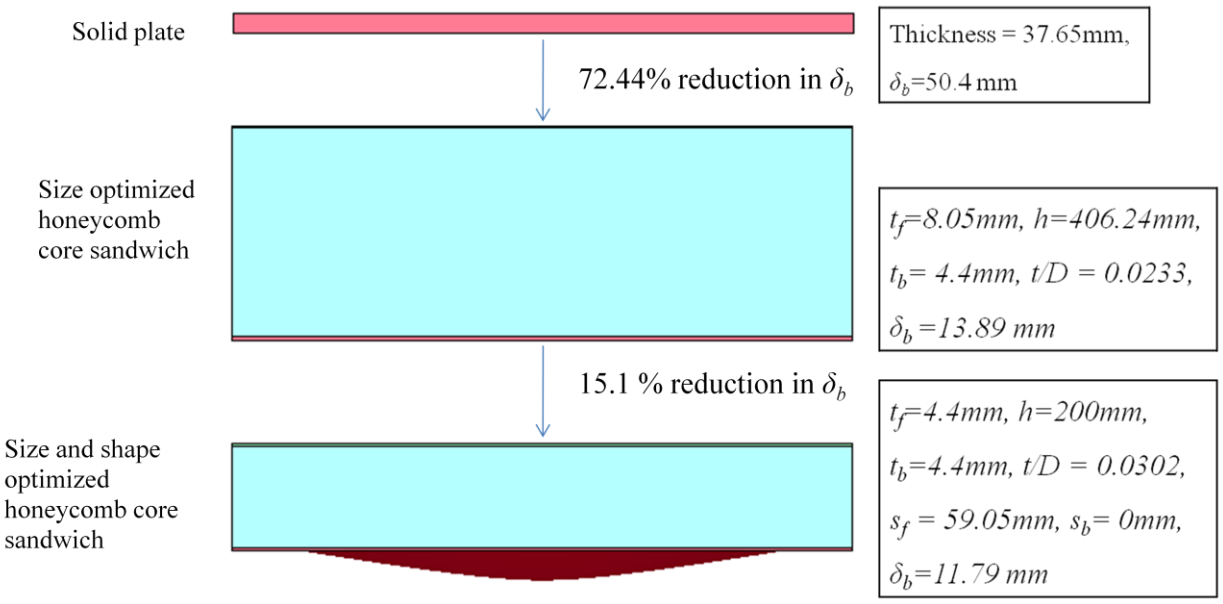

Figure **5-2**: Optimized sandwich panel of 150 kg mass for minimizing back face relative displacement δ_b (stiffener not shown)

Figure 5-3 compares the δ_b of the sandwich with the solid plate maximum Z-relative displacement. The maximum z-relative displacement and the amplitude of the oscillation of the solid plate are much higher than that of δ_b. Low δ_b can be attributed to the higher stiffness of the sandwich structure contributed by the core by maintaining space between the face plates. The characteristics of δ_b for size optimized sandwich panel and both size and shape optimized panel are similar. In the shape optimized panel, the bulge in the front face plate decreases the effective blast load by deflecting the blast wave, evident from the total Z-impulse plot in Figure 5-4. This bulge also increases the stiffness of the front face plate by which load transfer to the core becomes more uniform and reduces the negative effect of dishing deformation at center. The negative effect includes higher impulse and the lower moment of inertia at the center. The total Z-impulse for the size optimized sandwich is little higher than that of the solid (Figure 5-4). This is due to higher local deformation (dishing effect) of the front face plate.

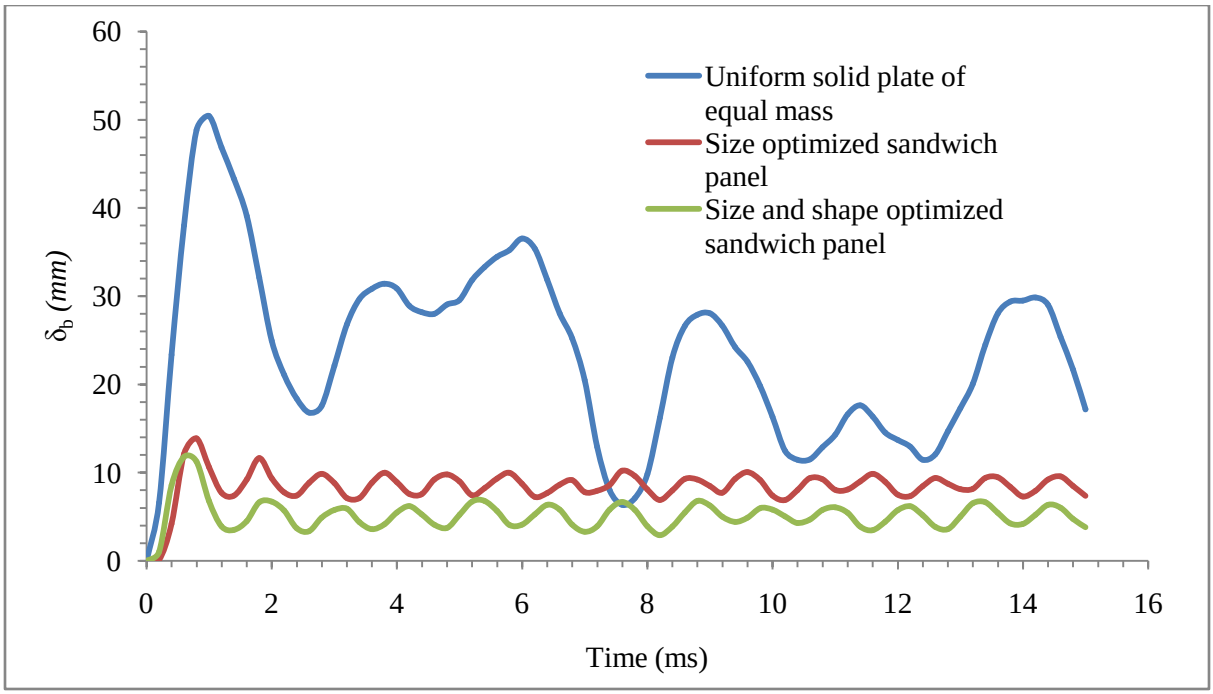

Figure **5-3**: Comparison of back face relative displacement δ_b for 150Kg mass of optimized sandwich and flat solid plate

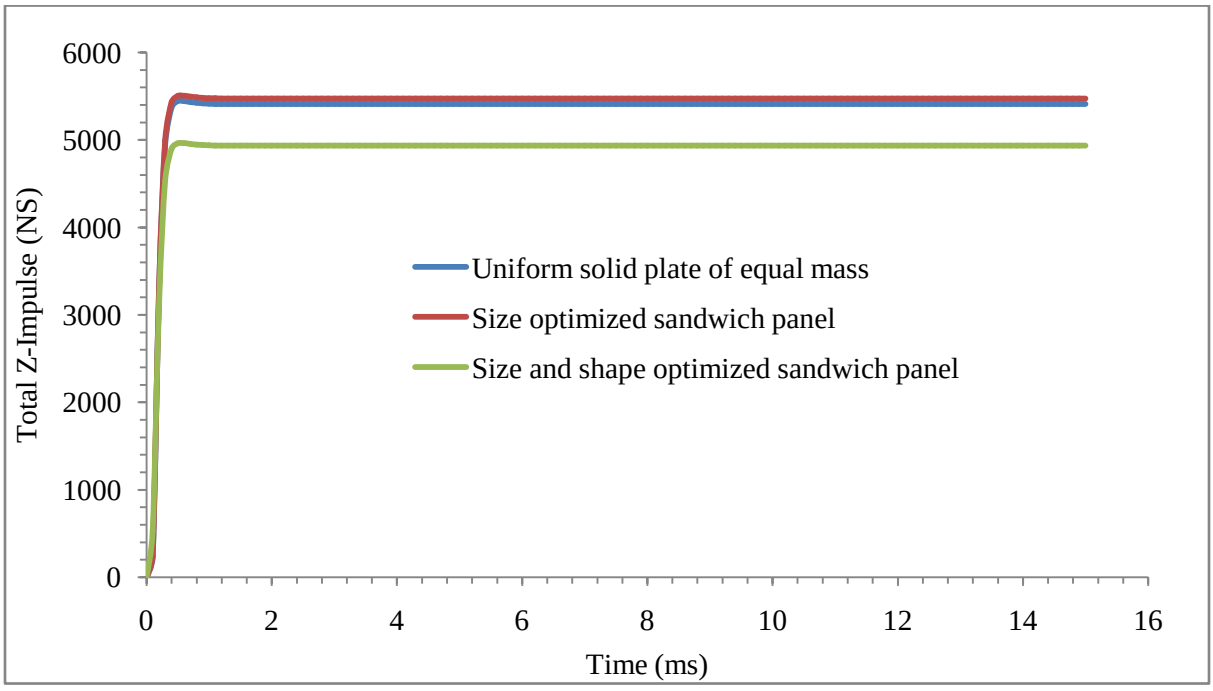

Figure **5-4**: Comparison of *total Z-impulse* corresponding to optimized δ_b

The maximum plastic strain of the solid plate is higher than the failure strain, where as it is well below the limit for the sandwich (Figure 5-5). The location of the maximum plastic strain is at the center of the back face plate for size optimized panel (Figure 5-6 (a)) and at the edge center of the back face plate for size and shape optimized panel (Figure 5-6 (b)). Relatively high plastic strain near the four edges is due to tied contact between the back face plate and the stiffener. The mass fraction in the front face plate, core and the back face plate are 0.241, 0. 666 and 0.093 respectively for size optimized panel and 0.467, 0.44 and 0.093 respectively for size and shape optimized panel. So optimizer tries to put higher mass in the front face plate (in the form of thickness and/or bulge) than the back face plate.

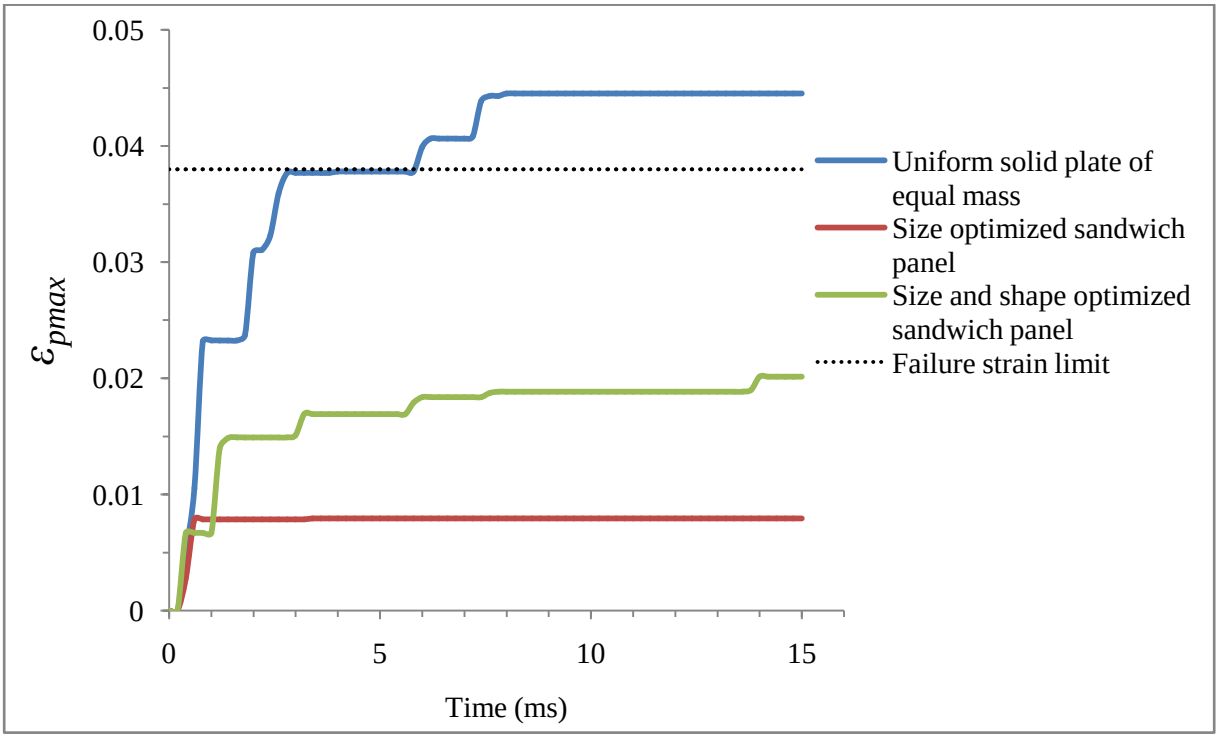

Figure **5-5**: Comparison of ε_{pmax} corresponding to optimized δ_b

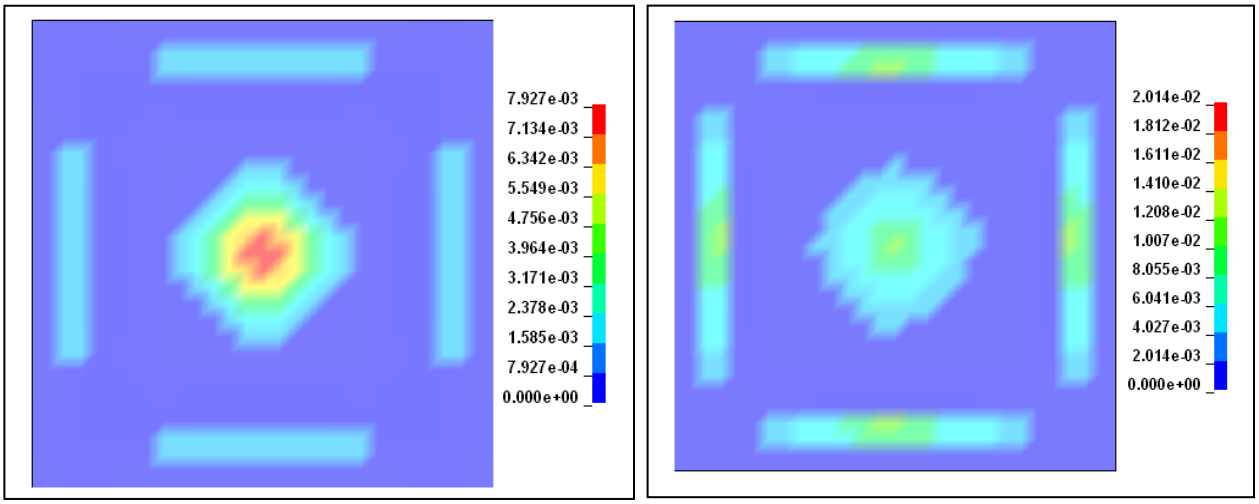

(a) (b)

Figure **5-6**: Plastic strain distribution in the back face plate corresponding to optimized δ_b

(a) size optimized and (b) size and shape optimized sandwich panel

Results with different mass limits

Tables 5-3 and 5-4 summarize the optimization results for different mass limits of the sandwich. Mass fraction of the front face plate increases with sandwich mass in terms of t_f in size optimization and s_f in simultaneous size and shape optimization. Thicker (stiffer) front face plate is good as explained in chapter-4. The optimizer always keeps the back face plate thickness at its lower limit. Higher *t/D* (means higher core density) reduces the dishing deformation and lowers δ_b. Larger core depth increases the overall stiffness of the sandwich and lowers δ_b. In size optimization, with sandwich mass, *h* doesn't changes much, but the core gets stiffer (due to increase of *t/D*). In size and shape optimization, with sandwich mass, *h and t/D* don't follow any particular trend. Maximum plastic is always in the back face plate (Table 5-2) since it is thinner or same to front face plate thickness and is fixed with stiffener.

Table **5-3**: Size optimization result from RSM for different mass of the sandwich (Mass is always active and all the units are in mm)

Sandwich Mass (Kg)	Optimized parameters					ε_{pmax}
	t_f	h	t_b	(t/D)	δ_b (Obj)	
100	4.4	387.97	4.4	0.0158	31.33	5.46e-3
125	4.4	402.12	4.4	0.0211	20.89	8.7e-3
150	8.056	406.24	4.4	0.0233	13.89	7.92e-3
175	12.344	407.57	4.4	0.025	9.78	7.08e-3
200	16.57	410.33	4.4	0.0267	8.18	5.53e-3
225	18	435.17	4.4	0.0294	6.83	2.89e-3
250	18	469.49	4.4	0.0322	5.89	2.85e-3

Table **5-4**: Size and shape optimization result from RSM for different mass of the sandwich (Mass is always active and all the units are in mm)

Sandwich Mass (Kg)	Optimized parameters							ε_{pmax}
	t_f	h	t_b	(t/D)	s_f	s_b	δ_b (Obj)	
100	4.4	270	4.4	0.0139	29.13	0	30.65	2e-3
125	4.4	200	4.4	0.0222	49.71	0	19.22	6.1e-3
150	4.4	200	4.4	0.0302	59.05	0	11.79	2e-2
175	4.4	260.28	4.4	0.0289	69.82	0	8.6	7.2e-3
200	4.4	337.21	4.4	0.0271	78.63	0	7.81	2e-3
225	4.4	407.54	4.4	0.0264	87.98	0	7.49	6.3e-4
250	4.4	249.14	4.4	0.0243	74.8	100	6.13	3.5e-5

5.2.1 Comparison of RSM and DE optimizers

DE violates the mass constraint by 5-15%. The sandwich masses 170.46 kg, 207.48 kg and 255.16 kg mentioned in the Table 5-5 are from the DE optimum result which corresponds to the defined mass constraint value 150 kg, 200 kg and 250 kg respectively. To compare the result for the same sandwich

mass, optimization in FMINCON is carried out for the revised mass 170.46 kg, 207.48 kg and 255.16 kg. It can be noted that 4.4 mm is used as the lower limit for t_f and t_b. The optimum δ_b obtained from RSM and DE matches very well. As noted in chapter-4, DE takes much more computation time. The RSM consistently tries to put higher mass in the front face plate and lower mass at the back face plate than DE does. DE produces higher *t/D* and lower *h* in the core than RSM does.

Table **5-5**: Size optimization for minimum δ_b using RSM and DE

(All the units are in mm)

M (Kg)		Optimized parameters					% mismatch in δ_b
		t_f	*h*	t_b	*(t/D)*	δ_b *(Obj)*	
170.46	RSM	11.8	400.1	4.4	0.0249	10.3	4.5
	DE	10.43	386.1	4.41	0.0271	10.78	
207.48	RSM	18	400.4	4.4	0.0278	7.93	2
	DE	11.75	372.9	4.56	0.0385	7.77	
255.16	RSM	18	476.3	4.4	0.0328	5.74	0.7
	DE	15.6	410.9	6.75	0.0381	5.7	

For simultaneous size and shape optimization comparison, optimization in RSM is again carried out at the mass DE gives at the end of the optimization. However, unlike in the pure sizing problem, here DE gives better result than RSM. The % mismatch between the optimum δ_b obtained from RSM and DE is up to 28.8. DE produces higher *t/D* and lower *h* in the core than the RSM. DE puts bulge in the back face plate at a lower mass of the sandwich where as FMINCON starts putting bulge at a higher mass of sandwich.

Table **5-6**: Size and shape optimization for minimum δ_b using RSM and DE

(All the units are in mm)

M (Kg)		Optimized parameters							% mismatch in δ_b
		t_f	h	t_b	(t/D)	s_f	s_b	δ_b *(Obj)*	
167.2	RSM	4.4	236.3	4.4	0.0295	67.3	0	9.45	7
	DE	4.42	210.13	4.42	0.0393	43.4	8	8.83	
212.02	RSM	4.4	385.2	4.4	0.0259	82.43	0	7.87	28.8
	DE	4.4	108	4.4	0.046	64.85	75.5	6.11	
258.04	RSM	4.4	400	4.4	0.017	74.98	100	5.43	26
	DE	4.4	102.9	4.9	0.046	98.75	99.68	4.3	

5.3 Size optimization results for minimizing a_b

Figure 5-7 shows the optimized sandwich panel for 150 kg mass and compares the optimized results with same mass solid plate. Size optimized sandwich panel results 83.5% reduction in a_b from an equal mass uniformly thick solid plate.

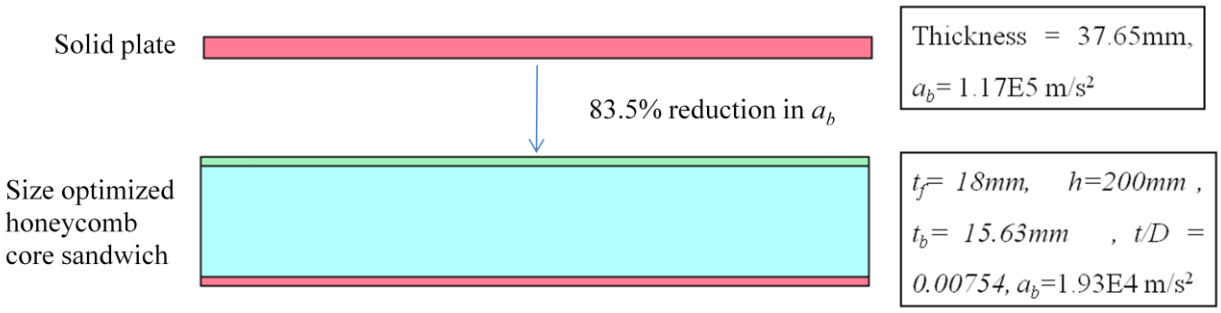

Figure **5-7**: Optimized sandwich panel of 150 kg mass for minimizing back face plate acceleration a_b (stiffener not shown)

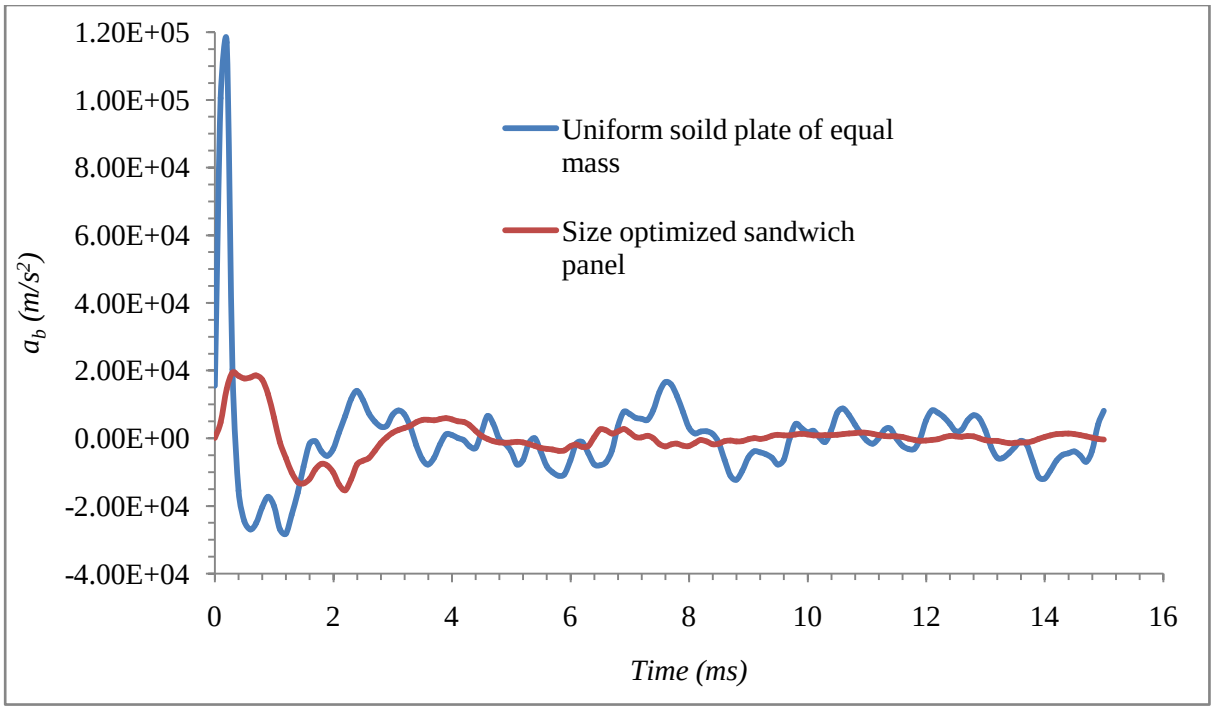

Figure **5-8**: Comparison of back face plate acceleration a_b for 150 kg mass of optimized sandwich and flat solid plate

Figure 5-8 compares the a_b of the sandwich with the solid plate *Z*-rigid body acceleration. The optimizer keeps *t/D* at its lower limit (0.00754). This soft core crushes and absorbs energy, thereby reducing the value of a_b. Size optimization results in $t_f = 18\ mm$ which is the upper limit value. This stiffer front face plate enables the effective utilization of the soft core (*t/D*=0.00754).

The total *Z*-impulse for the optimized sandwich is little higher than that of the solid (Figure 5-9). This is due to higher local deformation (dishing effect) of the front face plate. The location of the maximum plastic strain is at the center of the front face plate (Figure 5-10 and 11). The mass fraction in the front face plate, core and the back face plate are 0.48, 0.105 and 0.415 respectively.

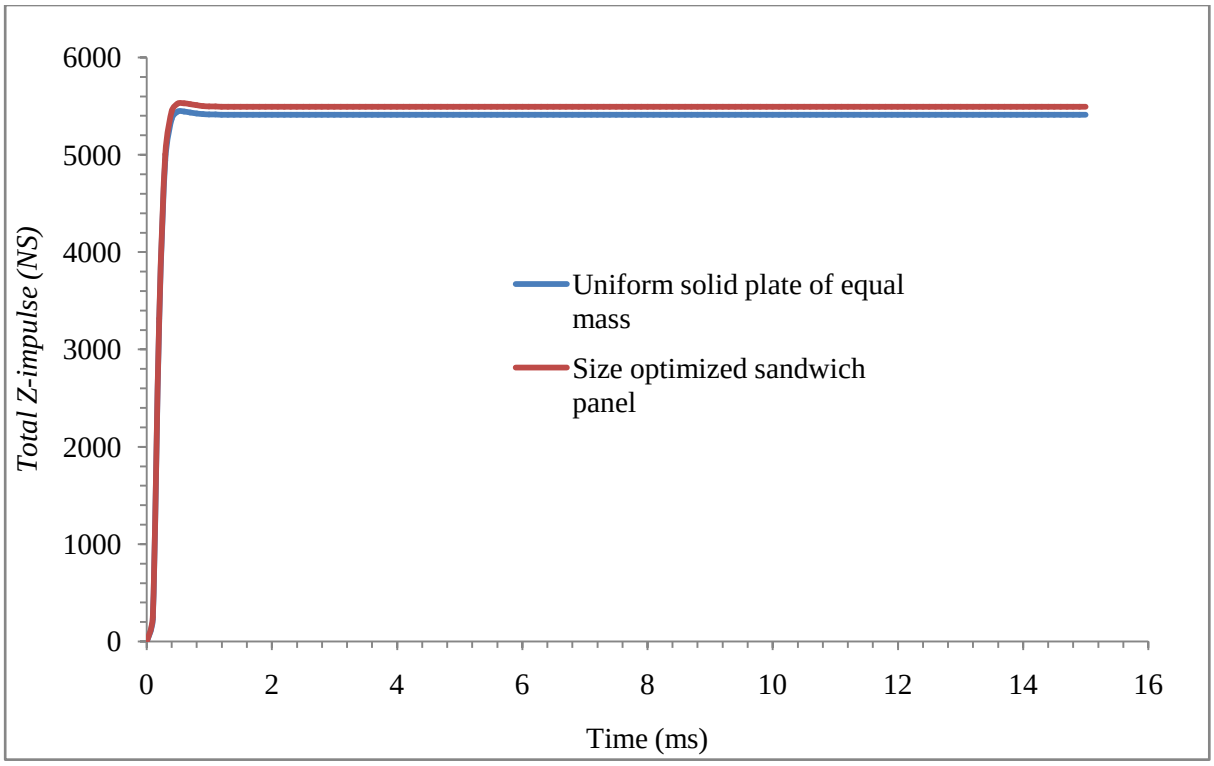

Figure **5-9**: Comparison of *total Z-impulse* corresponding to optimized a_b

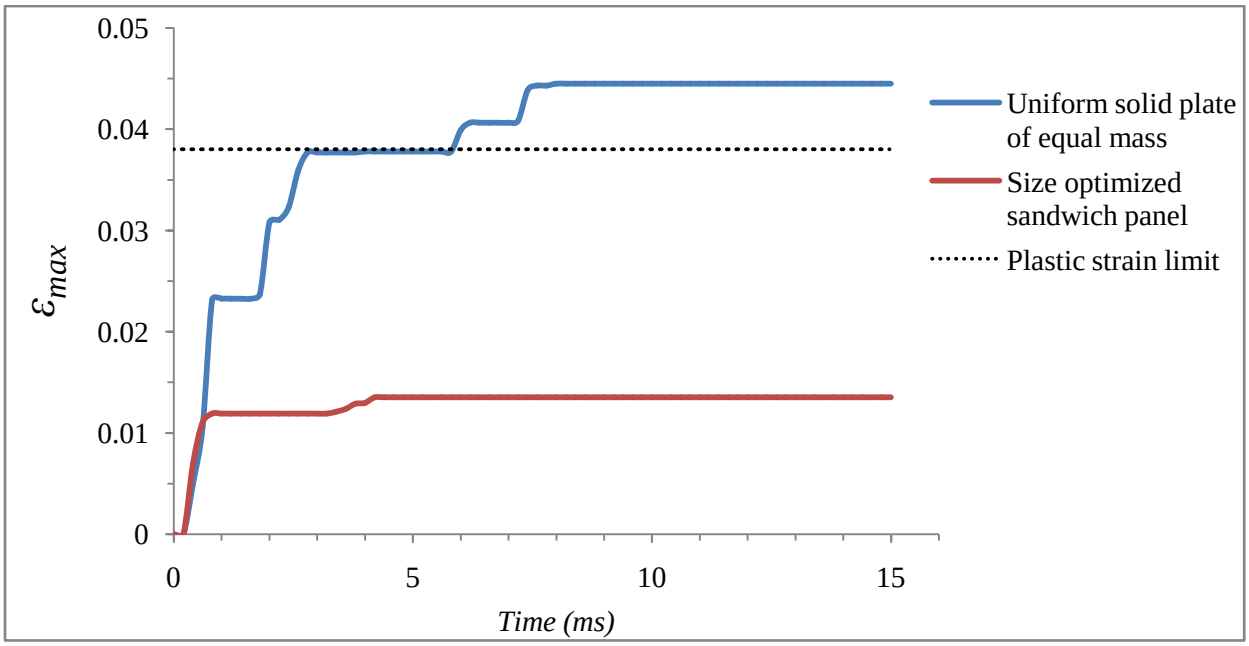

Figure **5-10**: Comparison of ε_{pmax} for 150 kg mass of optimized sandwich and flat solid plate

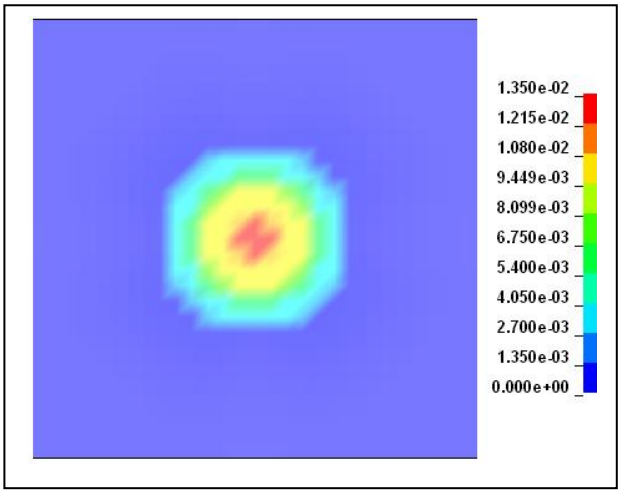

Figure **5-11**: Plastic strain distribution in the front face plate of 150 kg size optimized

Results with different mass limits

Tables 5-7 summarize the optimization results for different mass of the sandwich. Size optimized sandwich shows that both t_f and t_b increases with sandwich mass, but the size of the core remain same. t_f first reaches at its upper limit (Table 5-7) than t_b, which indicates that front face plate is more important in reducing the transmitted acceleration. The core density remains at its lower limit for every mass of sandwich. It can be observed that with increase in sandwich mass, optimizer preferably adds mass to the back face plate than the core. It can be explained that, the a_b not only depends upon the force transmitted to the back face plate but also on the back face plate mass. For same force, higher mass means less acceleration. So adding mass to back face plate reduces a_b better than adding mass to the core. Mass becomes inactive after 159.42 kg. Then any further addition of mass to the core in terms of h results higher a_b in the second peak.

Table **5-7**: Size optimization for minimizing a_b using RSM

(All the units are in mm, maximum plastic strain is always at the front face plate center)

M (kg)	Optimized parameters					ε_{pmax}	Mass Constraint
	t_f	h	t_b	(t/D)	a_b (Obj)		
100	14.49	200	6.59	0.00754	3.96e4	0.0184	Active
125	17.62	200	9.73	0.00754	2.82e4	0.0146	Active
150	18	200	15.63	0.00754	1.93e4	0.0135	Active
175	18	200	18	0.00754	1.7e4	0.0135	Inactive (159.42 kg)

5.4 Role of the honeycomb core for minimizing δ_b and a_b

Figure 5-12 shows that the maximum plastic strain in the honeycomb core, which is a direct indication of the amount of crushing of the core, corresponding to sizing optimization for minimizing δ_b is 0.055 (i.e. 5.5% crushing). On the other hand, maximum plastic strain is 0.573 (i.e. 57.3% crushing) for minimum a_b. It can also be noted that the t/D and the core depth h for minimum δ_b are higher than that of for minimum a_b. So high density (core density α t/D) and high depth core is required to minimize the δ_b by increasing the overall stiffness of the sandwich, whereas low density and minimum depth core (should be just sufficient to avoid densification, h=200mm is at lower bound) is required to minimize the a_b by absorbing blast energy through crushing. Also low density core crushes at lower stress and hence reduces the force transmission to the back face plate.

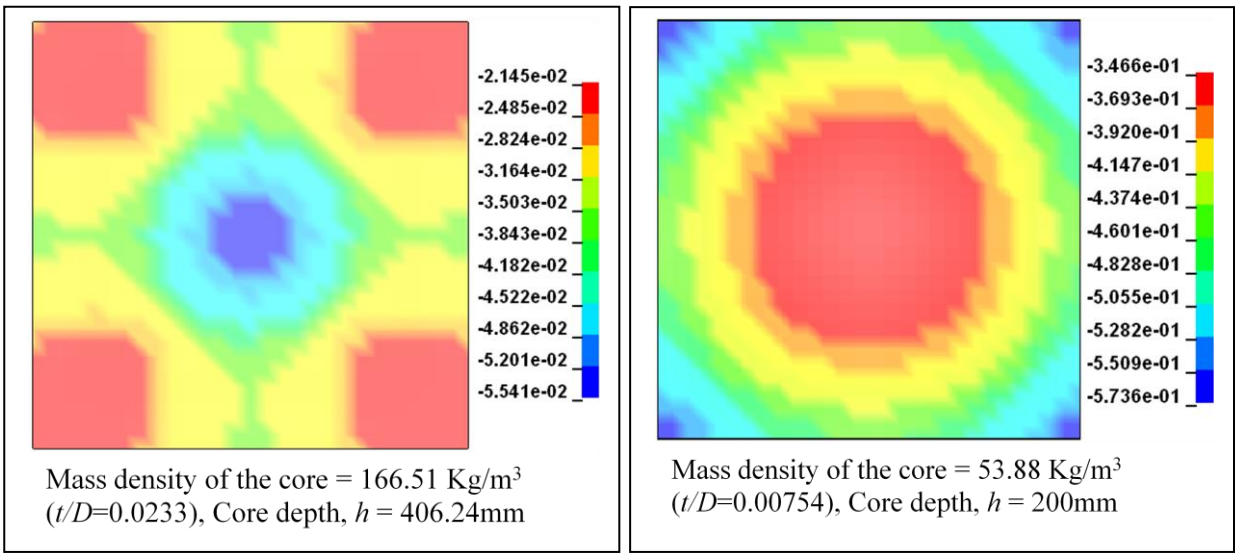

(a) **(b)**

Figure **5-12**: Plastic strain distribution along z-direction in the honeycomb core of 150 kg size optimized sandwich panel for minimizing (a) displacement, δ_b and (b) acceleration, a_b

5.5 Comparison of the optimized sandwich panel with shape-optimized solid plate

Here the optimized sandwich panel is compared with the shape optimized solid plate for both δ_b and a_b. Shape optimization of a solid plate for minimizing δ_b is carried out in DE as well as in RSM, both methods give exactly same result for the same mass. Also the shape optimization of the solid plate for minimizing δ_b and a_b gives same result. Figure 5-13 shows the optimized results for various cases. The mass 167.2 Kg refers to the final mass obtained from DE optimization in minimizing δ_b (in case of simultaneous size and shape optimization of sandwich panel) for 150Kg mass constraint limit. For valid comparison, the solid plate is optimized for the same mass using RSM. The sandwich panel is also optimized (only size) for the same mass in minimizing a_b, however the mass is inactive in this case. Same design limits are used on the thickness of the plate and bulge height.

Optimized solid plate has both front (active) and back bulge where as the sandwich panel (Figure 5-13 (b)) has only front bulge. The shape-optimized solid plate gives a lesser δ_b (Figure 5-14) than that of the size and shape optimized sandwich. Because of higher front bulge and lesser dishing deformation, total

Z-impulse in optimized solid plate is lesser than that of the optimized sandwich panel (Figure 5-16). Maximum plastic strain in the shape-optimized solid plate is lesser than that of the size and shape optimized sandwich (Figure 5-17). With higher bulge height limit, shape optimized solid plate gives even better result. Front bulge height increases up to 117 mm and thereafter it remains inactive even with higher bulge height limit.

Base thickness = 4.4mm, Front bulge height= 100mm, Back bulge height =73.74, optimized mass of the plate = 167.2 Kg, **δ_b = 8.77 mm, a_b = 7.97E4**

(a) Shape optimized solid plate for minimizing both δ_b *and* a_b

t_f = 4.42mm, h = 210.13m, t_b = 4.42mm, t/D = 0.0393, s_f = 43.4 mm, s_b = 8mm, optimized mass of the plate = 167.2 Kg, **δ_b = 8.83 mm**

(b) Size and shape optimized sandwich for minimizing δ_b

t_f=18mm, h=200mm, t_b=18mm, t/D=0.00754, Optimized mass of the plate (inactive) = 159.42 Kg, **a_b = 1.7E4 m/s^2**

(c) Size optimized sandwich for minimizing a_b

Figure **5-13**: Comparison of the optimized sandwich panel with shape-optimized solid plate

The size optimized sandwich panel reduces acceleration (a_b) by 78.7% than that of the shape optimized solid plate (Figure 5-15). Because of the flat front face plate and higher dishing deformation due to softer core, the total Z-impulse in size optimized sandwich panel is 21% higher than that of the shape optimized solid plate (Figure 5-16). Maximum plastic strain in the size optimized sandwich panel is lesser than that

of the shape optimized solid plate (Figure 5-17). All the design variables are active in size optimized sandwich panel (Figure 5-13 (c) and corresponding sandwich mass is 159.42 Kg (inactive). So there is a great potential in sandwich panel to reduce the acceleration further by both size and shape optimization.

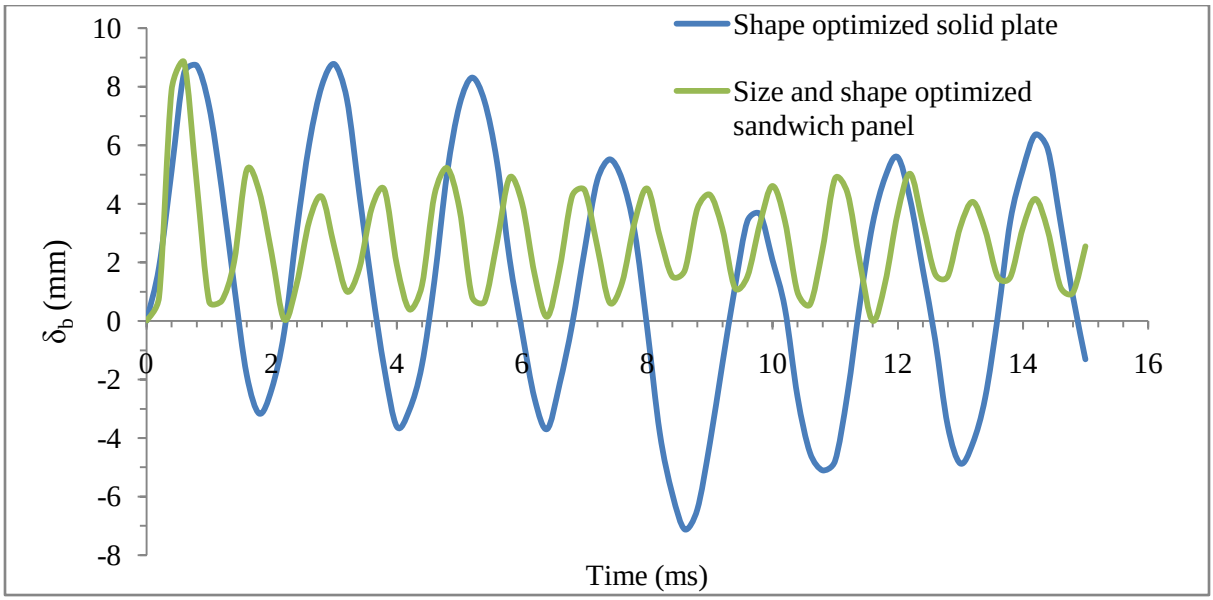

Figure **5-14**: Comparison of δ_b for shape optimized solid plate and shape-size optimized sandwich panel

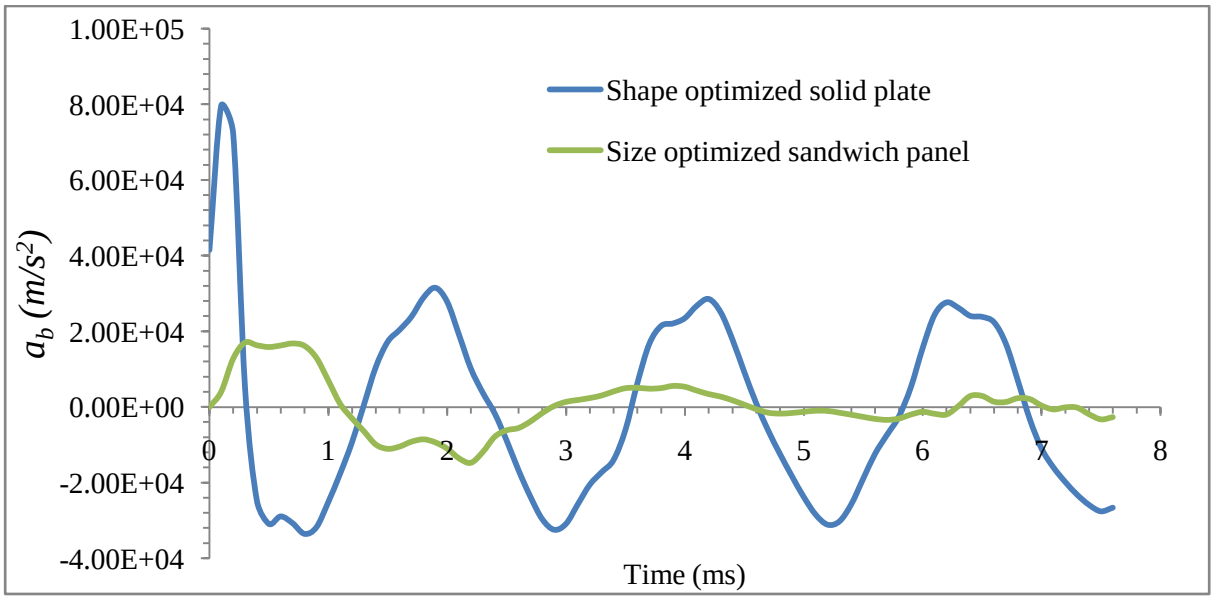

Figure **5-15**: Comparison of a_b for shape optimized solid plate and size optimized sandwich panel

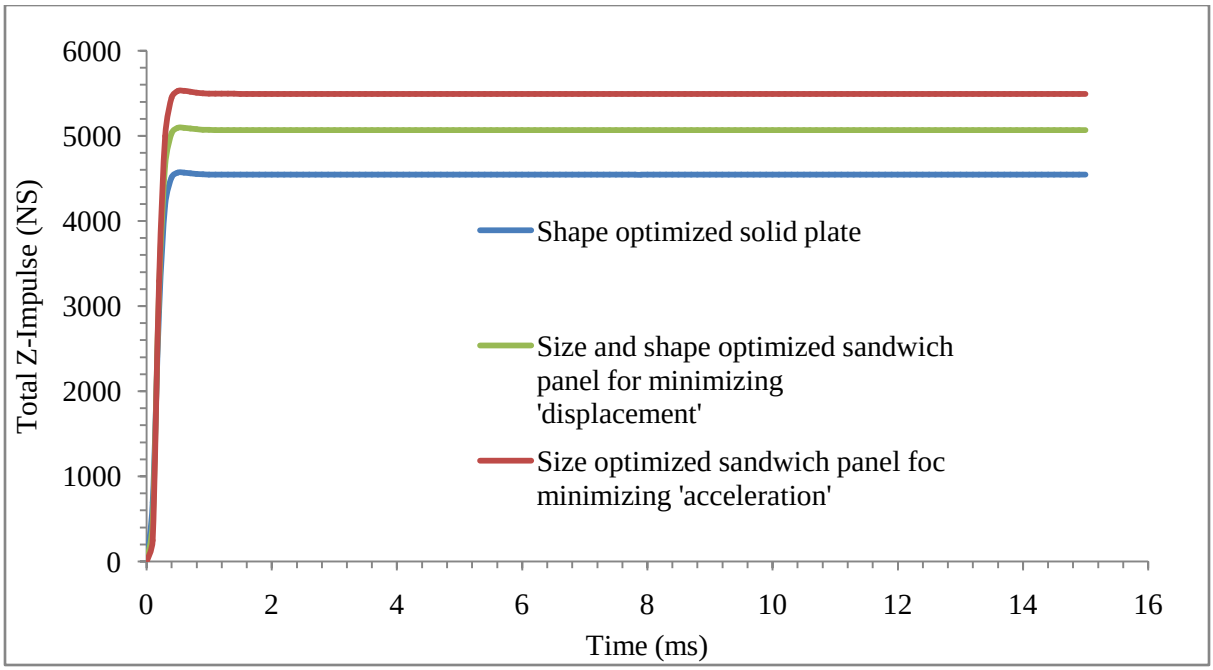

Figure **5-16**: Comparison of *total Z-impulse* between shape optimized solid plate and optimized sandwich panel

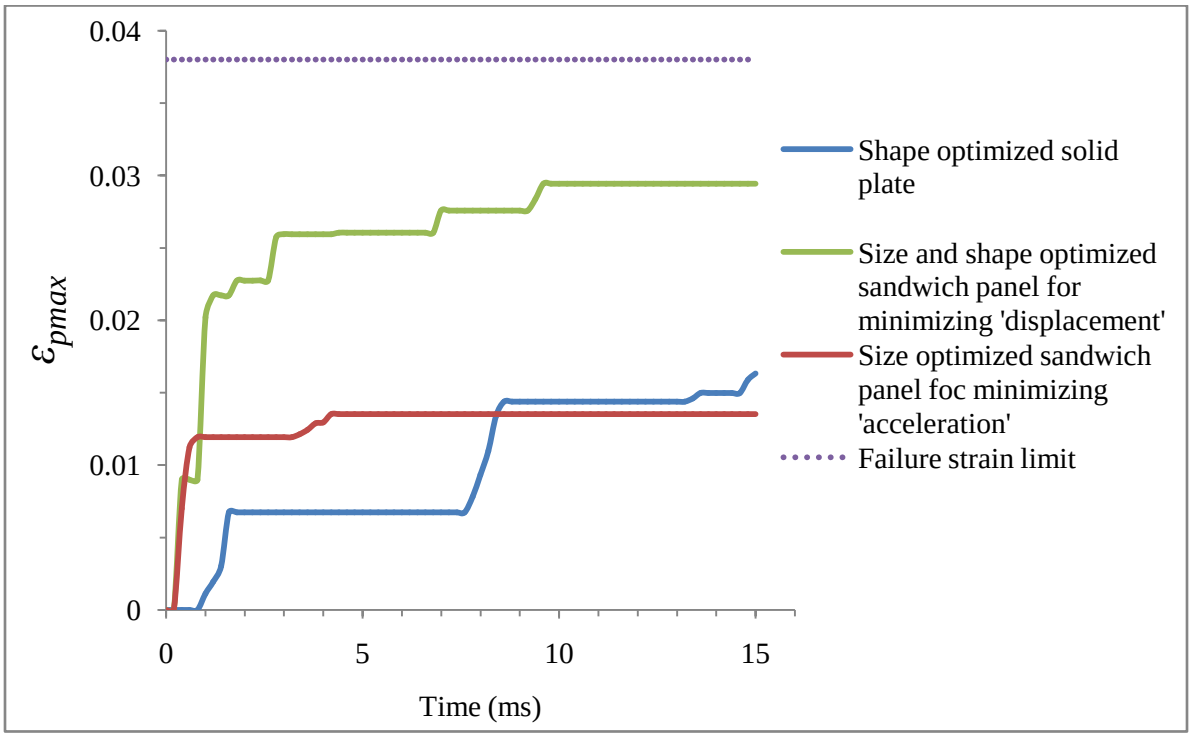

Figure **5-17**: Comparison of ε_{pmax} between shape optimized solid plate and optimized sandwich panel

Chapter-6

Conclusions and Future Work

The present research aims to optimize the honeycomb core sandwich panel to mitigate the effects of the blast load. Two independent design objectives, viz. back face plate deformation and back face plate rigid body acceleration are optimized subject to mass and plastic strain constraints. The optimization is carried out using two different methods, one based on response surface methodology (RSM) and the other based on direct use of differential evolution (DE). LS-DYNA is used for finite element simulations. RSM is based on Design Expert software to create response surfaces from sampled points based on central composite face centered design. The *MAT_CRUSHABLE_FOAM model in LS-DYNA is used to model the honeycomb core. Honeycomb core is modeled as a continuum solid structure with equivalent homogenized mechanical properties. The equivalent mechanical properties are determined by virtual testing method and parameterized in terms of the important honeycomb cell parameters. Virtual testing results have been corroborated with equations from the literature.

Considering δ_b minimization, results produce a stiffer front face plate which effectively transfers the blast load to a larger area of the core. Stiffer front face plate is achieved by thickness increase and/or a bulge. Back face plate thickness reaches as low a value as possible subject to plastic strain limit. Size and shape optimization results in a bulge on the back face plate at a higher mass constraint. Optimization produces a stiff core by increasing both t/D and h. That is, the mechanism of lowering the objective function is through stiffening the panel. Interestingly, for the same mass, the shape-optimized solid panel is equally effective as the honeycomb core sandwich panel.

Considering a_b minimization, results again produce a stiffer front face plate. Importantly, acceleration minimization produces a soft core by reducing t/D. That is, the mechanism of lowering the objective function here is energy absorption.

Honeycomb core sandwich structure proves to be very useful over the flat solid plate in reducing the deformation and transmitted acceleration to a great extent under blast loading. Shape optimized solid plate is found to be little better in reducing deformation than honeycomb core sandwich panel, where as the sandwich panel is much more effective in reducing the transmitted acceleration than a shape optimized solid plate. So the honeycomb core sandwich panel is a better choice over flat solid and shape optimized solid plate to mitigate the effects of air blast loading.

Future Work

Simultaneous size and shape optimization needs to be carried out in honeycomb core sandwich panel for acceleration minimization.

To consider the extreme limits of the design variable in design space, present work uses central composite face (CCF) centered method to create response equations. This method considers 3 levels of each factor. More investigations in to RSM should be done to produce accurate results for optimization of the back face plate acceleration especially using 5 levels of each factor.

Similar to the face plate shape, the honeycomb core shape can be introduced at the front face plate junction in the optimization. It is possible to manufacture shaped honeycomb although it is expensive.

In this study the back face plate deformation and acceleration of a sample sandwich panel model is minimized independently. The magnitude of the acceleration remains in the order of 1000g, where g is the acceleration due to gravity. However, the threshold for mild traumatic brain injury (TBI) is 50g. More realistic FE model can be developed which would keep the acceleration within the above limit and also defines the back face plate deformation limit for any practical application. In such case, minimizing the acceleration with a deformation limit would be more appropriate. The injuries caused to human body due to acceleration depend upon its magnitude as well as its time duration. Head injury criteria (HIC) and

chest injury criteria (CIC) which considers both magnitude and time can be used to investigate further in the optimization.

Bibliography

1. Argod,V., Nayak, S.K., Singh, A.K., Belegundu, A.D., *Shape optimization of solid isotropic plates to mitigate the effects of air blast loading*,
2. Argod,V., Belegundu,A.D., Aziz,A., Agrawala,V., Jain,R., and Rajan,S.D., *MPI-enabled Shape Optimization of Panels Subjected to Air Blast Loading*, Intl J of Simulation of multidisciplinary Design Optimization (2008)
3. Xue, Z. and Hutchinson, J.W., *A Comparative study of impulse-resistant metal sandwich plates*, International Journal of Impact Engineering, 30, 1283–1305 (2004)
4. Fleck, N.A. and Deshpande, V.S., *The Resistance of Clamped Sandwich Beams to Shock Loading*, vol. 71, J. of Applied Mechanics, Transactions of the ASME, 386-401, (2004)
5. Yen, C.F., Skaggs, R., Cheeseman, B.A., *Modeling of shock mitigation sandwich structures for blast protection*. The 3rd First International Conference on structural stability and dynamics, Kissimmee, Florida, June 19-22 (2005)
6. Hanssen, A.G., Enstock, L., and Langseth, M., *Close-range blast loading of aluminium foam panels. International journal of Impact Engineering* 27, 593-618 (2002)
7. Main, J.A. and Gazonas, G.A, *Uniaxial crushing of sandwich plates under air blast: Influence of mass distribution*, International Journal of Solids and Structures. 45, 2297–2321 (2008)
8. Chi., Y., Langdon., G.S., and Nurick., G.N., *The influence of core height and face plate thickness on the response of honeycomb sandwich panels subjected to blast loading.* Materials and Design 31, 1887-1899 (2010)
9. Zhu., Feng., Zhao., Longmao., Lu., Guoxing., and Wang., Zhihua., *Deformation and failure of blast-loaded metallic sandwich panels-Experimental investigations.* International journal of Impact Engineering 35, 937-951 (2008)
10. Zhu., Feng., Wang., Zhihua., Lu., Guoxing., and Zhao., Longmao., *Analytical investigation and optimal design of sandwich panels subjected to shock loading*. Materials and Design 30, 91-100 (2009)

11. Karagiozova., D., Nurick., G.N., and Langdon., G.S., *Behaviour of sandwich panels subject to intense air blasts-Parts 2: Numerical simulation.* Composite Structures 91, 442-450 (2009)
12. Yamashita., M., and Gotoh., M., *Impact behavior of honeycomb structures with various cell specifications- numerical simulation and experiment.* International journal of Impact Engineering 32, 618-630 (2005)
13. Wierzbicki., Tomasz., *Crushing analysis of metal honeycombs.* International journal of impact engineering 1, 157-174 (1983)
14. Zhang., J., and Ashby., M. F., *Buckling of honeycombs under in-plane biaxial stress.* International journal of mechanical sciences 34, 491-509 (1992)
15. Wu., Enboa., and Jiang., Wu-Shung., *Axial crushing of metallic honeycomb.* International journal of impact engineering 19, 439-456 (1997)
16. Hexcel Corp., *Hexweb honeycomb attributes and properties.* (1999).
17. Stuhmiller., James. H., *Blast injury translating research into operational medicine.* United states army medical research and material command, Maryland.
18. Bulmash, G.and Kingery, C.N *Computational Determination of blast wave pressure-time histories*, Computers in Engineering., Proceedings of the International Computers in Engineering Conference, Volume 2 p 343-347 (1986)
19. Sriram, R., Vaidya, U.K. and Kim, J., *Blast Impact response of aluminum foam sandwich composites*. Journal of Material Science 41,4023-4039 (2006)
20. LS-DYNA Keyword Manual version 971
21. Timoshenko, S. P. and Woinowsky-Krieger, S. *Theory of plates and shells,* Engineering Societies Monographs, New York: McGraw-Hill, 2nd edition (1959)
22. Myers, R., and Montgomery., D., (2009). *Response surface methodology- process and product optimization using designed experiments*, John Wiley & Sons, Inc.